IV. FINITE ELEMENT MODEL DEVELOPMENT AND VALIDATION

4.1   Introduction

The most common strong-post guardrail system in the United States is the G4(1S), which

is a steel post w-beam guardrail. This guardrail system is composed of 12-gauge w-beam

rails supported by W150x13.5 steel posts with W150x13.5 steel blockouts, as shown in

Figures 4.1 and 4.2. This guardrail successfully met the evaluation criteria of NCHRP

Report 230; however, it failed to meet the requirements of the current testing procedures

set forth in NCHRP Report 350.*(20)(21)* The G4(1S) was crash tested on June 9, 1994

under NCHRP Report 350 Test 3-11 conditions, i.e., impact by 2000P pickup at a

nominal speed and impact angle of 100-km/hr and 25-degrees, respectively.*(56)* The

guardrail system satisfied the structural adequacy and occupant risk factors criteria of

Report 350, but the vehicle rolled over onto its side after exiting the test installation and,

thus, failed the vehicle trajectory criteria.

The failure of the system was caused by the front wheel on the impact side snagging on

the guardrail posts. This is a common occurrence with other guardrail systems as well,

however, it is more likely in impacts with the G4(1S) due to the low torsional strength of

the W150x13.5 steel section blockouts, which collapse during impact and, thereby,

reduce the spacing between the vehicle and posts.*(56)* In an attempt to alleviate this

problem the W150x13.5 steel blockouts in the G4(1S) guardrail were replaced

with150x200 mm wood blockouts (*i.e.*, the type of blockout used in the G4(2W)

guardrail system), as shown in Figure 4.3

Figure 4.1: G4(1S) guardrail system.*(56)*
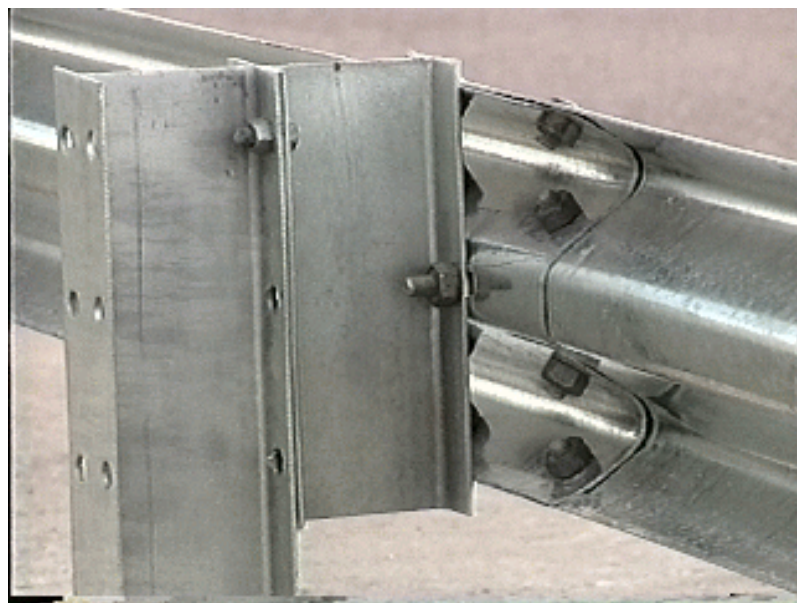
Figure 4.2: Close view of G4(1S) guardrail system.*(56)*

The modified G4(1S) guardrail with wood blockouts was successfully crash tested at Texas Transportation Institute (TTI test 405421-1) on November 16, 1995 under NCHRP Report 350 Test 3-11 impact conditions.*(57)* A sequence of snapshots from the crash test video is shown in Figure 4.4.

Figure 4.3: Modified G4(1S) with routed wood blockouts.*(57)*

Finite element analysis will be used to assess the performance of the modified G4(1S)

Figure 4.4: TTI test 405421-1 on the modified G4(1S) with wood blockouts.*(57)*

guardrail with wood blockouts in combination with various curb types. Section 4.2 below describes the modeling methodology used in the development of a finite element model of the modified G4(1S) guardrail system with wood blockouts. The modified NCAC C2500 reduced element pickup truck model will be used to simulate a crash test into the model of the modified G4(1S) guardrail for validation purposes. This vehicle model will also be used in the remainder of the study to simulate impacts into curbs and curb-and-barrier combinations. A brief description of the vehicle model is presented in section 4.3.

Section 4.4 will discuss the validation of the guardrail model by comparing the results to a full-scale crash test.

4.2   Modeling Methodology

Obtaining accurate simulations is dependent upon developing accurate models of each of the distinct components of the guardrail system and properly modeling their interaction with each other. Certain components of the system, however, must be modeled using rather simple methods (*e.g.*, springs and nodal constraints in lieu of bolted connections), due to the immense computational requirements of analyzing a complete guardrail system in geometric and material detail. Thus, an important consideration in developing a finite element model is balancing analysis time with the accuracy of the results such that realistic behavior is maintained in the simulation.

In order for a finite element analysis of a crash event to be computationally efficient a practical time-step for the analysis must be maintained (e.g., typically on the order of one- to three-microseconds - based on a combination of model size and current computation speed of computer hardware). If the various connections in the guardrail system, such as the w-beam splice and rail-to-post connections, were modeled in geometric detail, a very dense mesh in those local areas would be required in order to obtain the correct geometry of those components, as well as, to compute the high stress and strain concentrations in the local vicinity of the connections. It is typical to model connections using more simplistic modeling techniques such as spotwelds-with-failure or non-linear springs. In the impact region, however, where loads on the connections are

complex, it may be more practical to model the connections explicitly using a relatively

coarse mesh although the larger element size may result in a slightly over stiff response

of the connection. Other analysis simplifications in the model involve the boundary

conditions on the end of the guardrail model that simulate the anchor systems and also

the boundary conditions on the guardrail posts that simulate the posts' interaction with

soil.

Two models of the modified G4(1S) guardrail system were developed using the

preprocessor TrueGrid.*(58)* One model is relatively crude and utilizes many simplified

techniques for modeling connections. The second model is more complete and includes

explicit geometric modeling of the connections in the impact region, as well as, a more

complete model of the anchor system. The guardrail model is shown in Figure 4.5. The

model consists of 34.6 m of the guardrail system with nine 3.81-m sections of w-beam

rail, eighteen W150x13.5 steel posts spaced at 1.905 m, and eighteen 150 x 200-mm

wood blockouts. The modeling methodology for each component of the modified G4(1S)

guardrail system is provided in the following sections.

4.2.1 *W-Beam Guardrail*

<u>Geometry Modeling</u> The w-beam rail used in the modified G4(1S) guardrail is the

RWM02a, as designated in the AASHTO "A Guide to Standardized Highway Barrier

Hardware."*(59)* A drawing of the w-beam cross-section is shown in Figure 4.6. The

geometry of the finite element mesh of the w-beam must adhere, as closely as possible, to
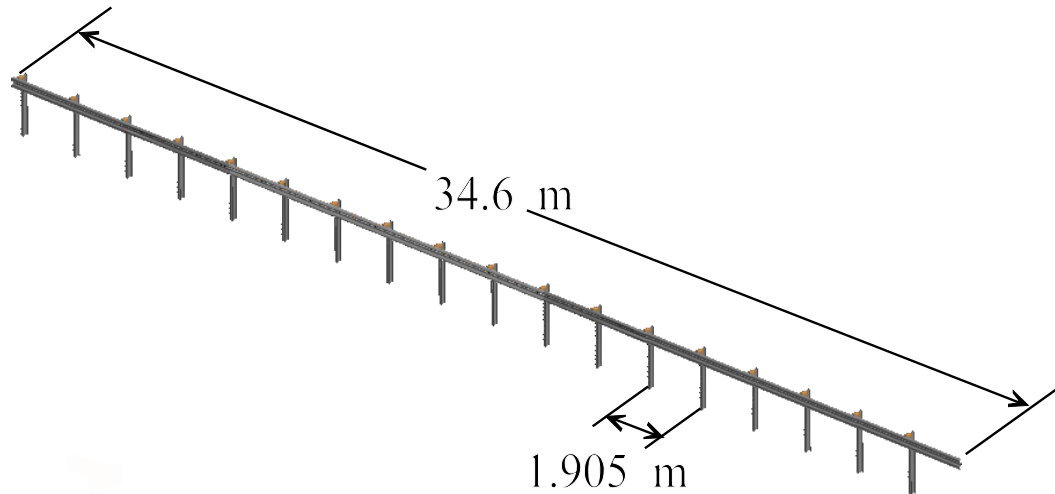
Figure 4.5: Finite element model of modified G4(1S) with wood blockouts.

the actual shape of the beam in order to accurately simulate the proper behavior of the w-beam during impact (*i.e.*, correct inertial properties and deformation modes). A comparison of the cross-section of the finite element mesh to the actual dimensions of the w-beam is shown in Figure 4.7, and a portion of the finite element mesh of the w-beam is shown in Figure 4.8. There are 24 elements defining the cross-section of w-beam mesh, which is adequate for simulating the response of the w-beam while maintaining a reasonable time-step in the analysis. The average element aspect ratio in the w-beam model is 2 to 1. The smallest element dimension is 14 mm in the w-beam cross-section, and the largest dimension is 48 mm in the axial direction of the beam. The largest aspect ratio is thus 3.4 to 1.

Material Modeling - The key to success using finite elements is having accurate material property information to input into the model. For instance, the yield point of a material

83

2   81

57

42

59

24 R
(TYP)

10°±1°

℄ POST BOLT SLOT
(20 x 65)

83

312
(±5)

14

194

24 R
(TYP)

55°
(TYP)

55°

156

55°

21

10 R

℄ 24x30 SLOTS

SHEET
THICKNESS

27

TOL
(-0,+5)

1994

2-SPACE W-BEAM GUARDRAIL

RWM02a-b

SHEET NO.	REF. NO.
3 of 4	RE-3-73
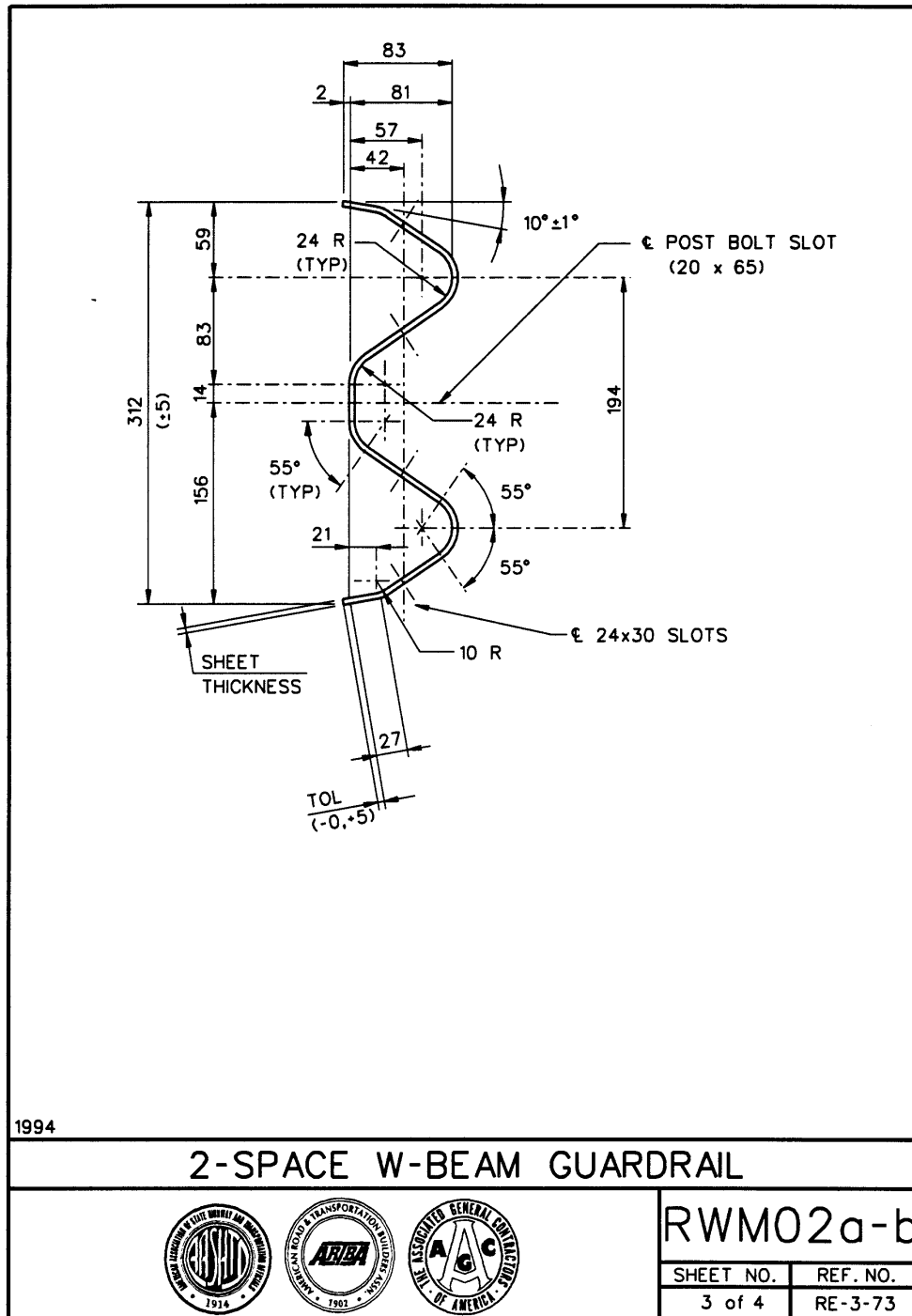
Figure 4. 6: Drawing of the w-beam cross-section *(59)*

W-Beam Cross-Section View   Finite Element Mesh
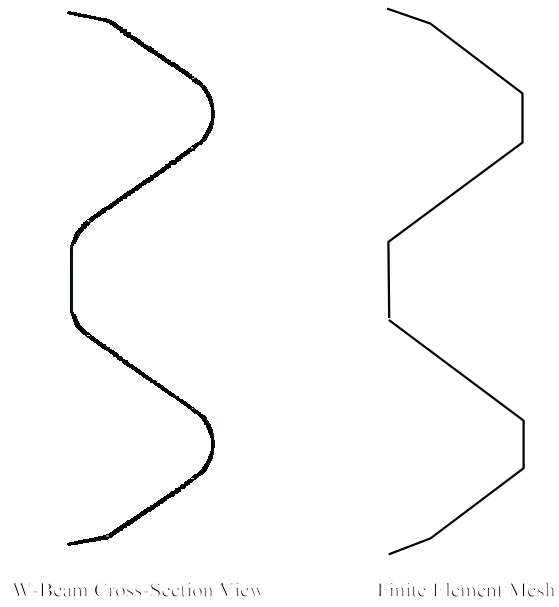
Figure 4.7:   Cross-section views of the w-
               beam and finite element mesh for
               geometrical comparison.
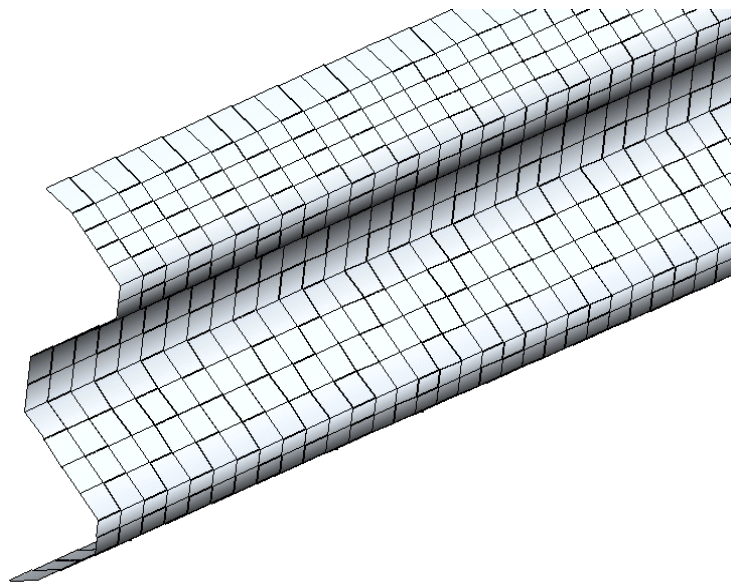
Figure 4.8: Finite element mesh of w-beam in impact region of model.

obtained from design handbooks usually provides a minimum value, which is likely less than the actual yield stress. This value is acceptable for design purposes, but, in order to simulate results from physical tests, accurate material properties must be used in the analysis. Wright and Ray published a paper in 1996 characterizing material properties for certain structural steels for use in LS-DYNA, namely AASHTO M-180, AASHTO M-183, and AASHTO A-499.*(60)* The w-beam rail material is classified as AASHTO M-180 Class A Type II. The material properties of the w-beam are modeled using material type 24 in LS-DYNA (*i.e.*, piecewise linear elasto-plastic material with kinematic strain hardening and strain-rate effects) as given by Wright and Ray.   The material property input data used in the model of the w-beam is provided in Table 4.1.

Table 4.1:   LS-DYNA material properties for modeling AASHTO M-180 steel using material type 24. *(60)*

Density (Mg/mm^3)							7.86E-09
Young's Modulus (MPa)							200.0E+03
Poisson's Ratio							0.30
Yield Stress (MPa)							415.0
Strain Rate Effects				Cowper Simons model*(61)* with D = 100.4 p = 4.9			
Increments of Strain	0.0	0.020	0.080	0.165	0.330	0.495	0.660	1.00
Increments of Stress (MPa)	0.0	415.0	548.0	585.0	591.0	595.0	600.0	600.0

Element Formulation - The element formulation used in the models was the Belytschko-Lin-Tsay (BT) shell element with three integration points through the thickness. The BT element is much more computationally efficient than the other under-integrated elements

such as the Hughes-Liu (HL) shell element. For a shell element with three through-the-thickness integration points the BT element requires 435 mathematical operations compared to 2,440 mathematical operations for the under integrated HL element and 21,219 mathematical operations for the selectively reduced integration HL element.*(62)* The disadvantages of using the BT element are the increased potential of zero-energy modes (hourglassing) and the fact that the element formulation does not account for out-of-plane warping which is likely to occur in large deformation regions of the mesh.

The zero-energy-modes can be repressed using hourglass control methods available in LS-DYNA. There are basically two types of hourglass control in LS-DYNA: viscous form and stiffness form. If hourglassing is a serious problem the stiffness form does a much better job of keeping the hourglass modes in check; however, it can result in a stiffer response from the model. The viscous hourglass form (type 2) works best when hourglass modes are not excessive. The stiffness hourglass control method was used in the model.

The effects of hourglass modes and warping can also be reduced by using a relatively fine mesh in the large deformation regions. One must be careful, however, when creating mesh that is more dense in one area than another, because a dense-mesh region will be less stiff than a neighboring coarse-mesh region. Thus, biasing mesh density may pre-define the deformation region and mode of deformation.

Strain-Rate Effects - The strain rate effects were incorporated in the model using a load

105

curve to scale the stress magnitude as a function of strain-rate using the Cowper-

Symonds empirical strain rate model. The empirical relationship developed by Cowper-

Symonds is:

$$\frac{\sigma}{\sigma_0} = 1 + \left(\frac{d\varepsilon/dt}{D} \right)^{1/p}$$

where σ_0 is the quasi-static stress, $d\varepsilon/dt$ is the strain rate, and σ is the resulting rate-

affected dynamic stress. The constants, D and p, are material properties. Typical values

for the strain rate properties of mild steel are D=40.4 and p=5.0.*(63)* These values give

reasonable results for steel that has been annealed.*(64)* As the strength of steel increases

it becomes less sensitive to strain rate. From the work of Wright and Ray the strain rate

properties of AASHTO M-180 steel are: D=100.4 and p=4.9.*(60)* These values were used

in the above equation to generate the load curve scaling factor for use in the finite

element model. Table 4.2 lists the values used in the model.

Application - The w-beam model presented here has been used effectively in previous

studies of impact with other guardrail systems.*(48)(52)* The results of a finite element

analysis of the G4(2W) guardrail, which uses the same w-beam rail as the G4(1S), is

compared to the results of a full-scale crash test conducted by TTI in Figure 4.9.*(39)(48)*

The model adequately simulates the proper deflections and deformation modes of the rail

during impact.

Table 4.2: Load curve defining scale factor for stress vs strain rate

Strain Rate	Stress Scale Factor $1+\left(\dfrac{d\varepsilon/dt}{D}\right)^{1/p}$
0.0	1.0
1.0	1.390
2.0	1.450
3.0	1.488
4.0	1.518
5.0	1.542
6.0	1.563
7.0	1.581
8.0	1.597
9.0	1.611
10.	1.625
11.	1.637
12.	1.648
13.	1.659
14.	1.667
15.	1.678
16.	1.687
17.	1.696
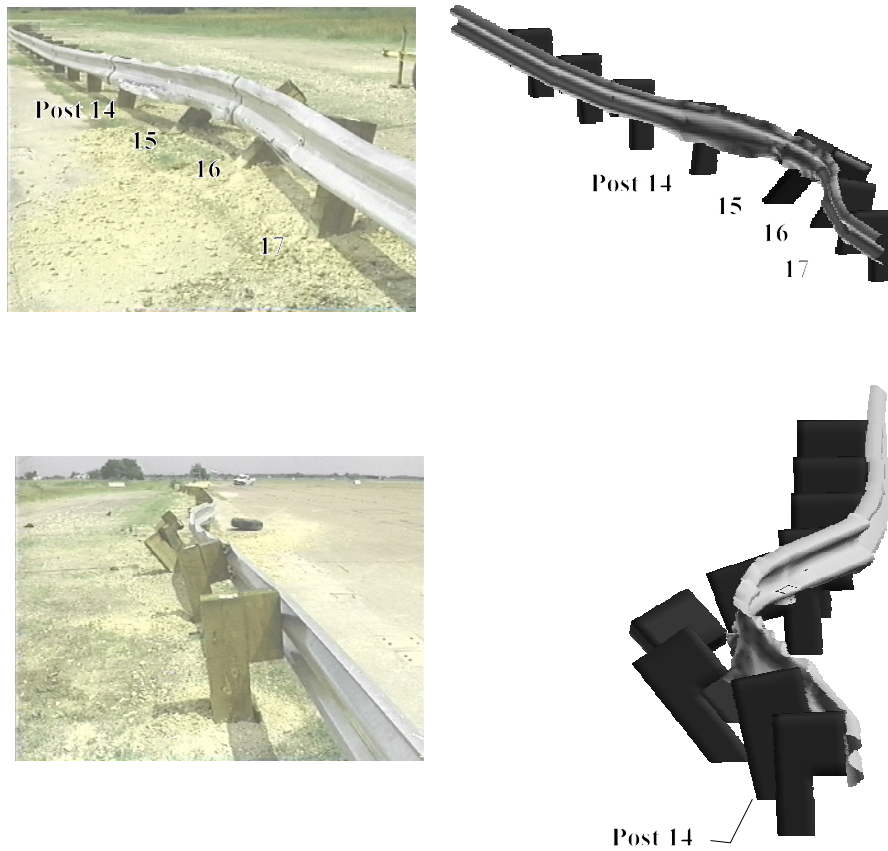
Figure 4.9:   The G4(2W) guardrail after test 471470-26 (left) and G4(2W)
finite element simulation results(right).*(48)(57)*

In the regions of the guardrail system up-stream and down-stream of the impact location,

the deformation mode of the w-beam rail is that of simple extension (*i.e.,* the w-beam is

in "pure" tension) and can be modeled with a less refined mesh density. Since the axial

stress in the rail governs its behavior in these regions, the cross-section shape of the w-

beam is also of less importance to the analysis results and only the cross-sectional area

and material properties need be considered with any accuracy. With this in mind, the

model of the w-beam, both up-stream and down-stream of the impact region, was

modeled with a relatively coarse mesh and "crude" representation of the w-beam shape, while retaining the proper cross-sectional area of the w-beam rail, as shown in Figure 4.10.
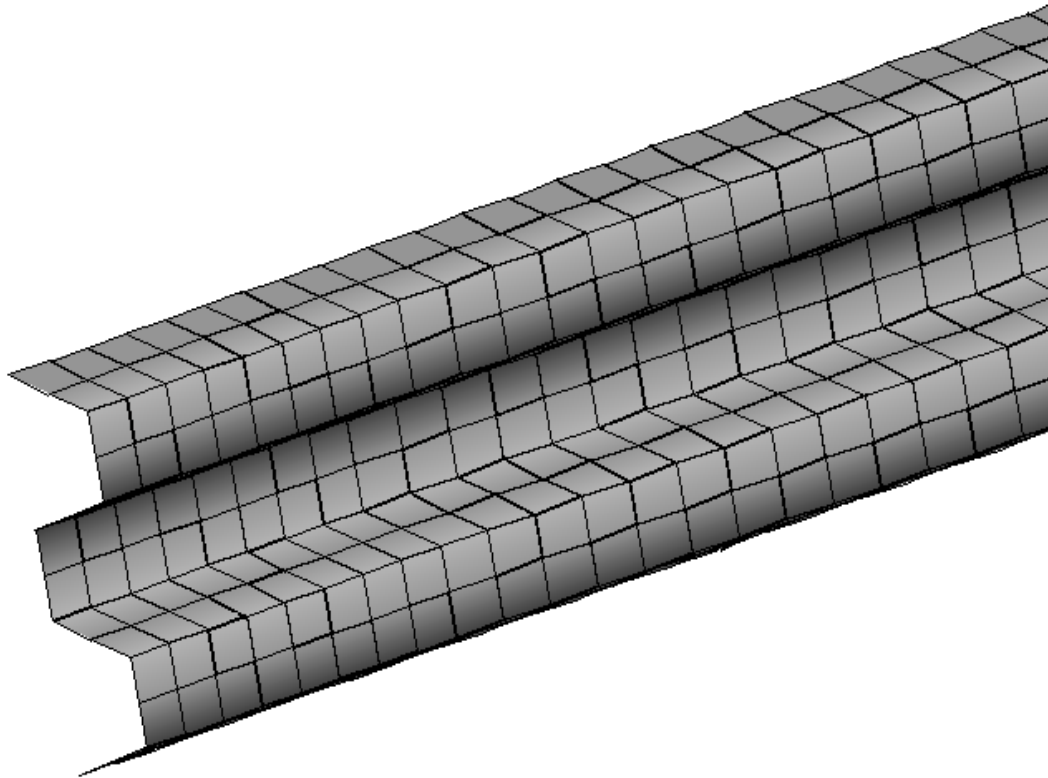
Figure 4.10: Finite element mesh of w-beam in non-impact regions of the model

4.2.2   W-Beam Splice Connection

Another important consideration in modeling the w-beam rails is the splice connections that fasten the individual rail sections together. The splice is sometimes the point of structural failure during impact.*(29)* W-beam guardrails are connected by overlapping the

ends of the rail sections and clamping them together using eight 16-mm diameter bolts
and nuts, as shown in Figure 4.11. In a study conducted by Ray *et al.* the performance of
w-beam splices were analyzed using the results of full-scale crash tests, laboratory
experiments and finite element simulation.*(50)(51)* It was concluded in their study that
w-beam splices should be located at the mid-span between posts to eliminate their
interaction with guardrail posts. In the modified G4(1S) and many other guardrails and
guardrail terminal systems, the splice is located at the posts where the splice is subjected
to a combination of axial guardrail tension, torsion in the guardrail section about its
longitudinal axis, and lateral bending of the splice against the guardrail posts.
Incorporating failure into the model of the splice connection would require a very fine
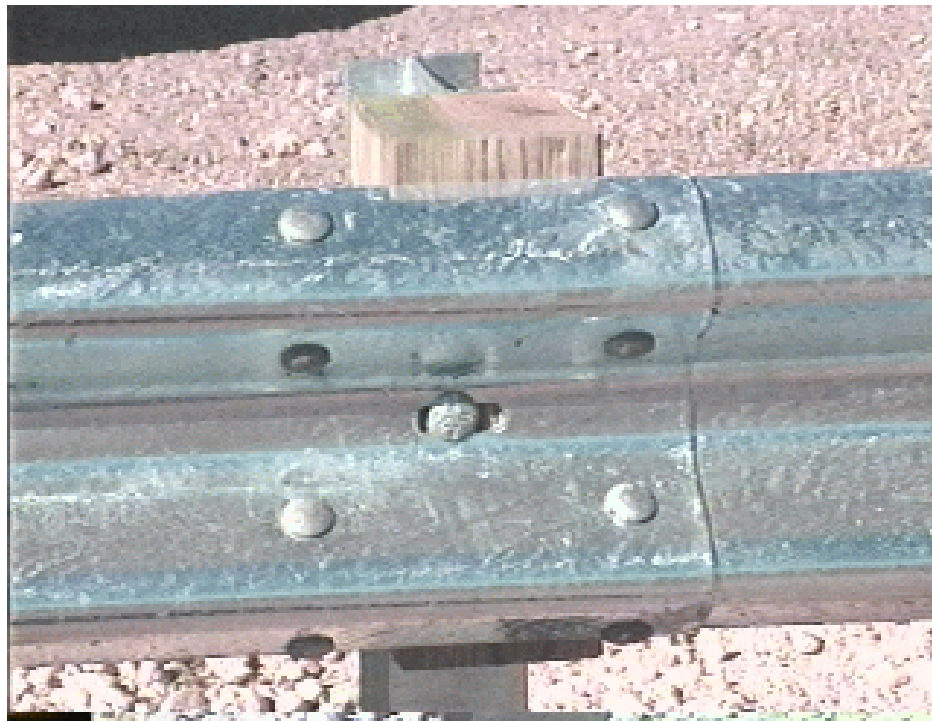
Figure 4.11:   Guardrail splice connection in the modified G4(1S)
guardrail.*(57)*

mesh in order to capture the local stress concentrations around the splice bolt

connections, as demonstrated by Ray *et al.(49)* The finite element model of the splice

and guardrail used in their study is shown in Figure 4.12. Using such a fine mesh in the

current model would require a time-step on the order of 0.1 microseconds and is

obviously not feasible in the analysis of a full-scale impact event which lasts 0.6 to 1.2

seconds (*e.g.*, the analysis would require 6,000,000 to 12,500,000 time-steps to complete

the simulation). Thus, a more simplistic modeling technique must be used to simulate the

bolted connections such as nodal rigid body spot-welds, non-linear springs or modeling
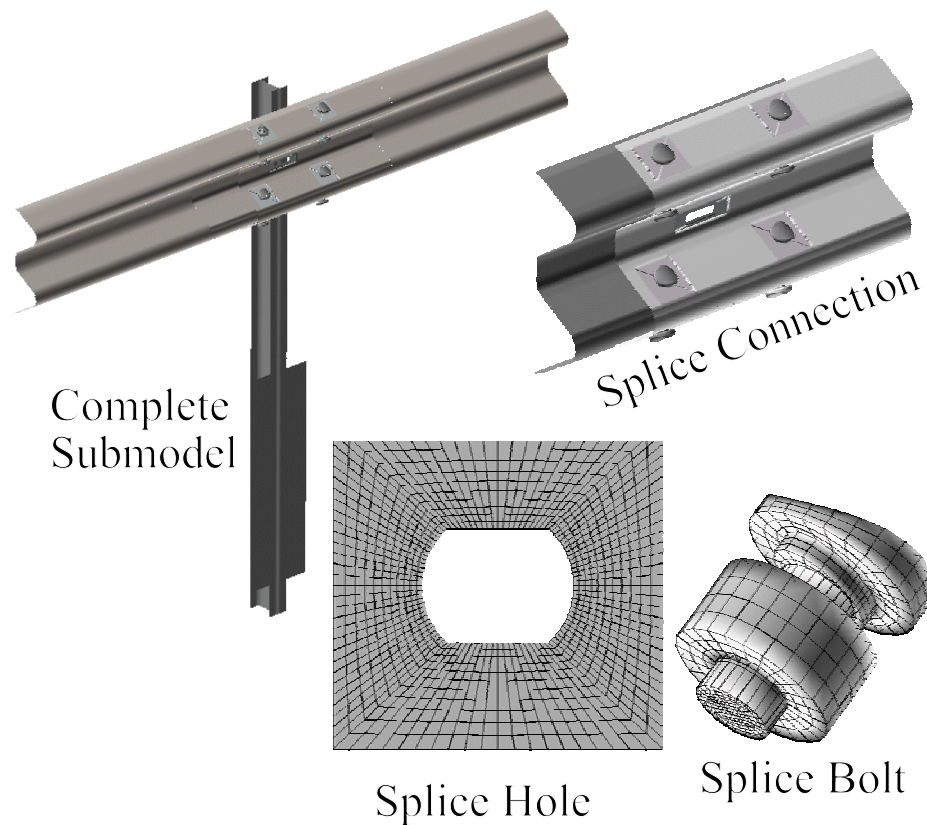
Figure 4.12:   Components of the finite element model of a weak-post w-beam
                  guardrail splice used in Ray *et al. (51)*

the connection in geometric detail with a relatively coarse mesh. Nodal rigid bodies would not be able to simulate the relative movement of the two w-beam sections in the splice, since they are rigid connections and are, therefore, not recommended.

When the splice is in uniaxial loading the most appropriate method of connecting the w-beams together would be to use non-linear springs with a force-displacement relationship defined such that the correct axial displacement of the splice is obtained for a given tensile load in the w-beam. This is especially important in the upstream and downstream regions of the guardrail model away from the impact zone, where the rail is in "pure" tension. In the impact zone where the loading on the splice is more complicated, it may be necessary to model the bolted connection explicitly, even though this will require a relatively coarse mesh of the splice holes for computational reasons. When a more thorough analysis is needed it is common practice to perform a full-scale simulation of a guardrail system and use the results of the analysis to identify the critical regions in the system that may have the potential for failure. Sub-models of these components in these critical regions can then be developed with appropriate mesh densities so that they can be thoroughly assessed using loading conditions obtained from the full-scale simulation.

In the study by Engstrand the force-displacement relationship of the splice connection in pure tension was determined.(49) This information, however, was only used in their study to show that the mode of failure of a splice connection in pure tension was quite different than the failures experienced in full-scale crash tests. Figure 4.13 was taken

from Engstrand's thesis, and shows the results of the laboratory tests from that study. The

force-displacement relationship of the splice shown in table 4.3 was obtained from the

test results and was implemented into the current model.

Table 4.3: Axial force-deflection properties of splice connection from Engstrand. *(49)*

Displacement (mm)	Force (N)
0.	0.
2.	200,000
8.	340,000
10.	360,000
16.	400,000
18.	400,000
25.	390,000
30.	360,000

The finite element mesh of the splice connection in the current model is shown in Figure

4.14a. The two sections will not fit readily together due to the shape of the w-beam

cross-section, therefore, the two sections of rail are initially offset from each other in the

model and are clamped together in the analysis by defining the nonlinear springs having

initial tension (*i.e.*, clamping force). Upon the start of the analysis the springs contract

and clamp the two sections together as shown in Figure 4.14b.

The spring element definition in LS-DYNA has an option that allows one to specify a
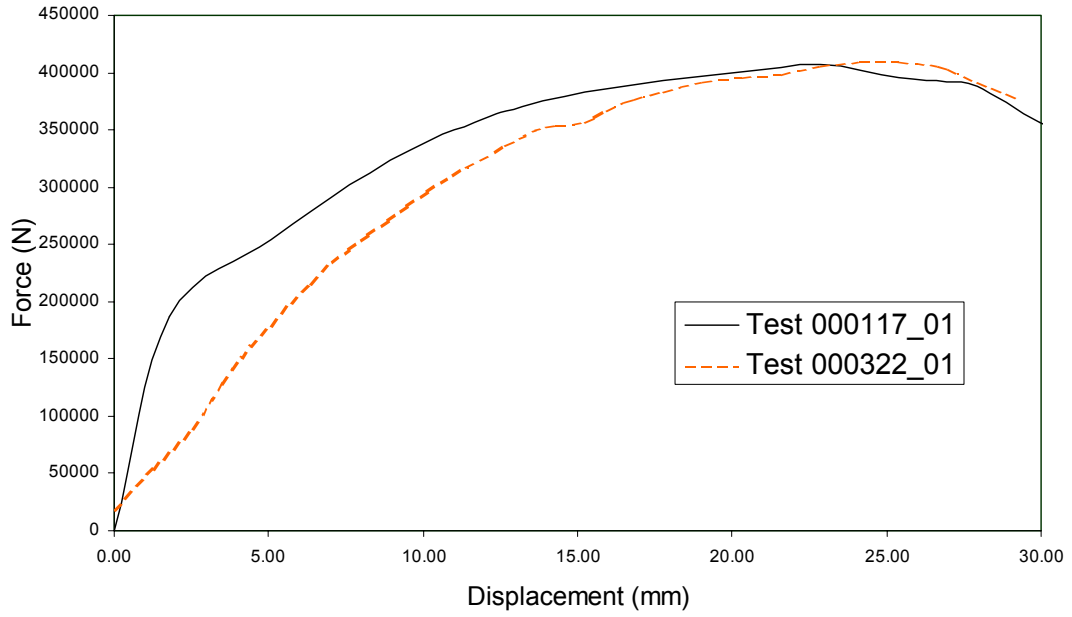
Figure 4.13: Axial force-displacement graphs from uniaxial tension tests of guardrail splices.*(49)*
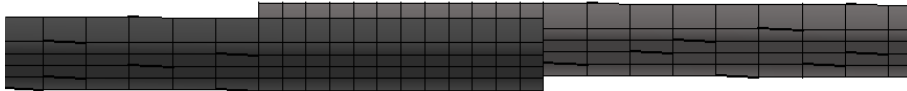
a

b

Figure 4.14: a) initial position of splice prior to start of simulation b) position of splice just after start of simulation due to clamping springs.

specific direction in which the springs act. In previous models of splice connections two sets of springs were used: one set to clamp the splice together and another set to simulate tensile forces in the splice in the axial direction of the w-beam. The problem with this method is that during impact the orientation of the splices change. The w-beam in the model is oriented such that the axial direction of the w-beam coincides with the global x-direction. So, if the clamping and tensioning springs of the splice are defined to act in the global y-direction and x-direction, respectively, then during impact the local coordinate directions of the splice may no longer coincide with that of the global directions, and the simulated splice connections will be in error. This problem could be corrected by defining a local coordinate system at each bolt connection, and defining the springs to act in the local coordinates directions. However, defining a local coordinate system for every bolted connection (*i.e.*, eight at each splice connection) would be tedious at best.

In the current model only one set of springs is used to both clamp the two rail sections together and to provide the appropriate tensile resistance in the splice. These springs act in the direction along the axis of the individual springs. The following definition of the splice connection assumes that once the two rail sections are clamped together, they remain in contact with each other throughout the remainder of the analysis. Furthermore, it is assumed that when clamping the rails together each of the bolts are tightened such that there is a tension of 10 kN in each bolt (note: this value is only an assumption but it serves to keep the rails from separating in the lateral direction of the splice). The force-deflection relationship in the longitudinal direction of the w-beam (tensile force) is

shown both graphically and in table form in Figure 4.15.

The springs contract approximately 12-13 mm when clamping the splice together due to the initial offset of the two w-beam sections. The force-displacement curve of Figure 4.15, therefore, must be shifted to the left 13 mm so that, when the splice is clamped, the net force in each of the springs is 10 kN. The thickness of the two w-beam rails must also be considered since the w-beam is modeled using shell elements where the element nodes are located at the centerline of the w-beam material in the thickness direction. When the splice is clamped, the length of the spring will be approximately 2.67-mm (*i.e.*, the distance from center-to-center of the two w-beam rail thicknesses). Referring to Figure 4.16, as node 2 moves in the local x-direction the spring stretches by amount ΔL, where

$$\Delta L = (\Delta x^2 + L_0^2)^{\frac{1}{2}} - L_0$$

and $L_0 = 2.67$ mm.

**Figure 4.15**: Force-deflection relationship of splice connection in the longitudinal direction of w-beam.
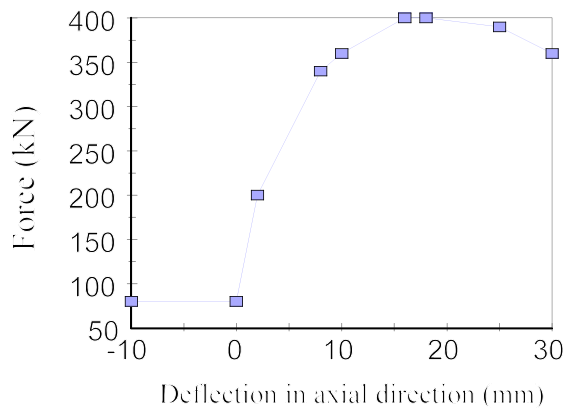
Deflection of spring (mm)	Force (kN)
-10.	80
0	200
2.	340
8.	360
10.	400
16.	400
18.	390
25.	360

116
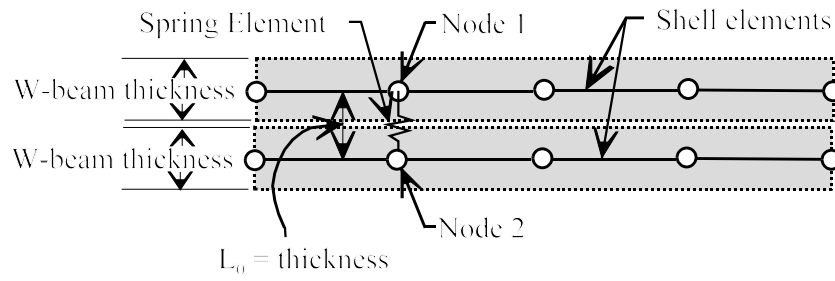
A) Initial clamped position
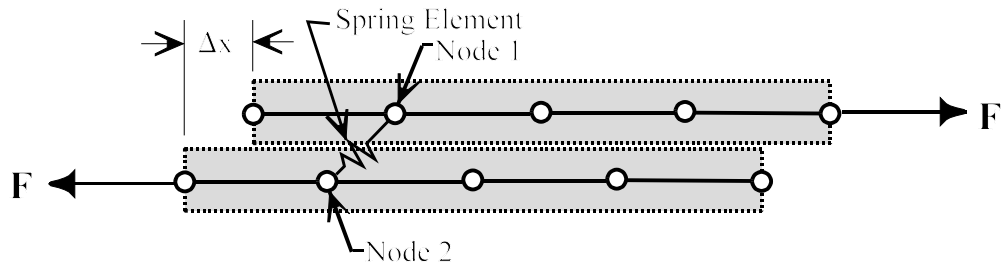
B) Deformed position due to tensile force F
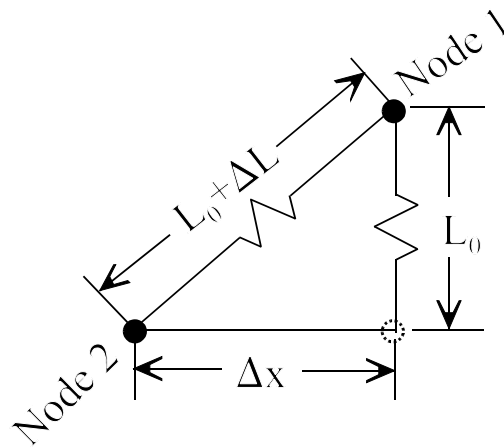
C) detail of spring element orientation in deformed position

Figure 4.16:   Schematic representation of longitudinal spring deflection in splice.

117

For example, when the w-beam is in tension, a relative displacement of 2 mm between the two rail sections corresponds to a spring deflection of 0.667 mm in the spring. Using the relationship of longitudinal splice displacement, Δx, and spring elongation displacement, ΔL, in the above equation, and noting that the spring contracted approximately 13 mm in the clamping phase, the following spring force-displacement relationship, shown in Figure 4.17, can be obtained for each of the eight springs in the splice connection. To verify the accuracy of the splice modeling technique a finite element model was developed of two w-beam rails that were spliced together using non-linear springs as just defined with properties given in Figure 4.17. A displacement-time history was applied to the ends of the rails and the resulting force-deflection response of the simulated splice connection is compared to the test results from Engstrand in Figure 4.18.*(49)*
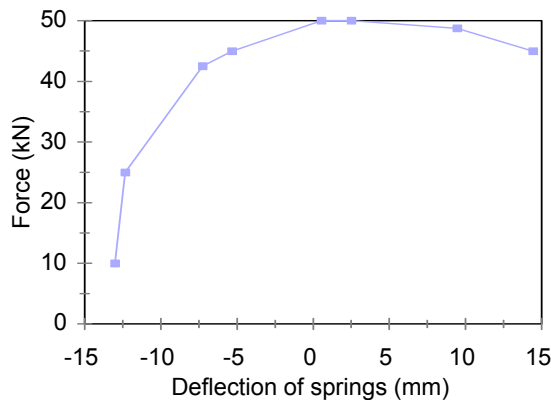

Figure 4.17: Force deflection relationship of individual springs in splice.

| Deflection of spring (mm)	Force (kN)
-13.0	80/8
-12.33	200/8
-7.24	340/8
-5.32	360/8
0.55	400/8
2.53	400/8
9.47	390/8
14.45	360/8
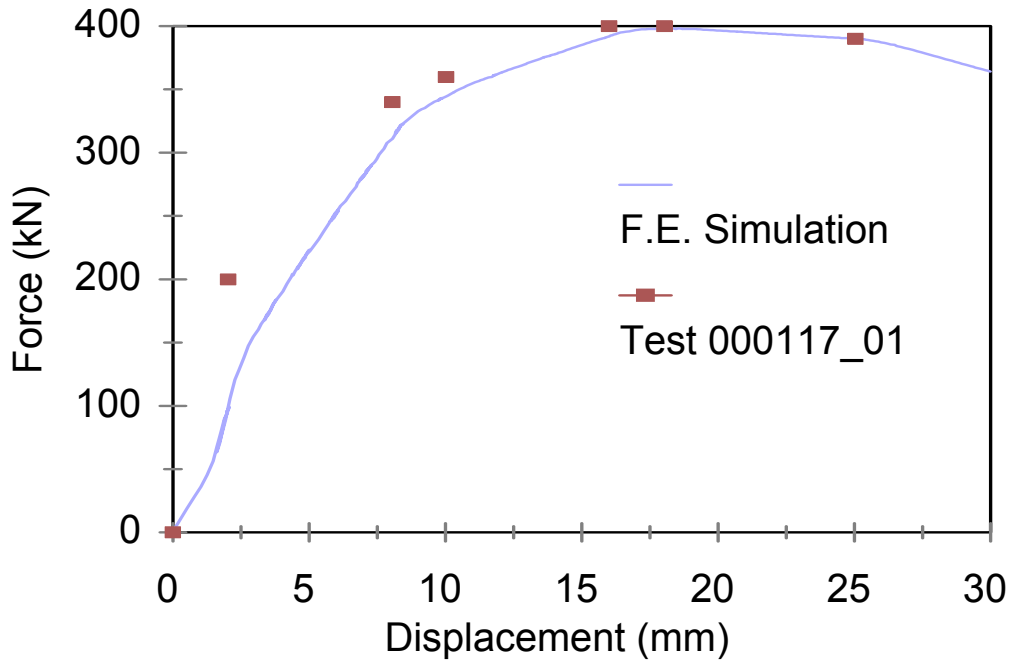
Figure 4.18:   Force-displacement response of simulated splice connection and laboratory test.

From preliminary simulations of a full-scale impact event with the model (which will be discussed in more detail in section 4.3) it was determined that a more explicit model of the bolted connections in the splice may be warranted in the impact region of the model. In the non-impact regions, where the w-beam rail is in pure tension, the non-linear spring model is still considered to be the most accurate method for simulating the connection. A second model of the guardrail was developed in which the exact geometry of the splice holes in the w-beam and the splice bolts were modeled explicitly in the impact region of the guardrail model, as shown in Figure 4.19. The splice was modeled by giving the over-lapping w-beam sections an initial offset. At the start of the simulations the nuts of the
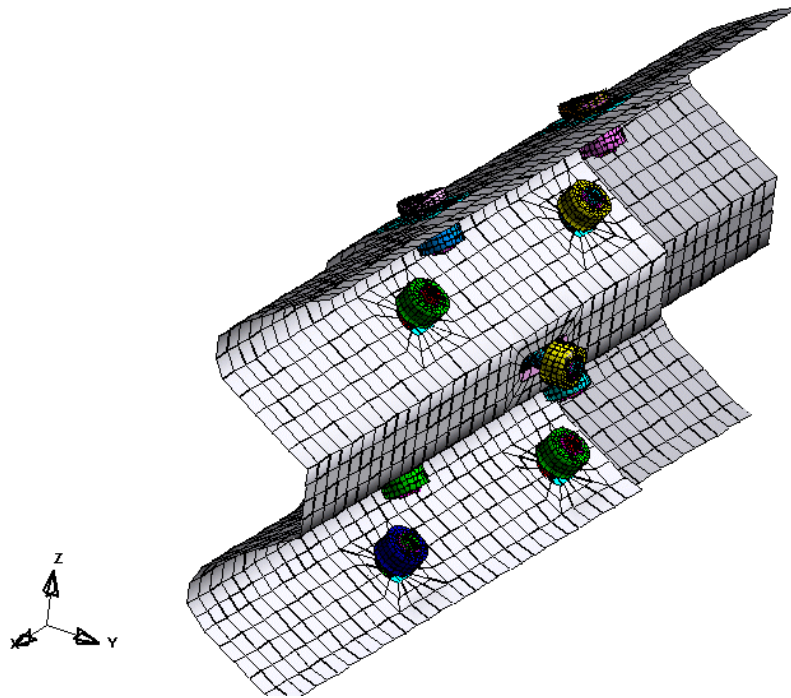
Figure 4.19:   Splice model in the impact region of the guardrail (Model 2).

splice bolts clamp the two sections together. The mesh of the w-beam is relatively coarse for modeling this connection, thus it is expected that the stress concentrations in the w-beam at the bolted connections will be in some error (the connection will be more stiff and the computed stresses will be lower than would be in an actual splice connection). The model, however, will provide very useful information regarding the deformations in the splice, which can be used to determine if a more thorough analysis need be conducted to assess potential splice failure.

4.2.3 Guardrail Posts

The posts used in the modified G4(1S) guardrail system are the PWE01, which are W150x13.5 structural shape. A drawing of the PWE01 post was taken from the AASHTO Barrier Hardware Guide and is shown in Figure 4.20.(59) Two finite element models were developed of the post: one with a relatively fine mesh for use in impact regions of the guardrail and another with a coarse mesh for use in the non-impact regions. The finite element meshes for these two models are shown in Figures 4.21 and 4.22, respectively. A fine mesh was necessary in the impact region due to the large deformations of those posts during impact. The W150x13.5 posts are very weak in torsion and tend to twist during impact which, consequently, reduces the lateral bending stiffness of the posts. This event may significantly affect the redirective performance of the guardrail and must be accurately simulated in the model. A simple parametric study was conducted to determine the proper element type, mesh density and number of through thickness integration points for the shell elements. A summary of the results from that study are presented here.

The material for the W150x13.5 structural shape is classified as AASHTO M-183. The material properties of the post are modeled using material type 24 in LS-DYNA as given by Wright and Ray.(60) The material property input data used in the model of the w-beam is provided in Table 4.4.

DESIGNATOR	L	D	E
PWE01	1830	1100	52
PWE02	1980	1250	52
PWE03	1980	1153	149
PWE04	2060	1173	149

W150x13.5
STRUCTURAL
SHAPE

X — · — — · — X

150

OPTIONAL HOLES IN
OPPOSITE FLANGE
FOR MEDIAN BARRIER
APPLICATIONS.

OPTIONAL HOLE FOR
W-BEAM RUBRAIL.

GROUND LINE

60 20

128

128

222

SIDE

FRONT

1994

WIDE-FLANGE GUARDRAIL POST

PWE01-04

SHEET NO.	REF. NO.
1 of 2	P-10-79
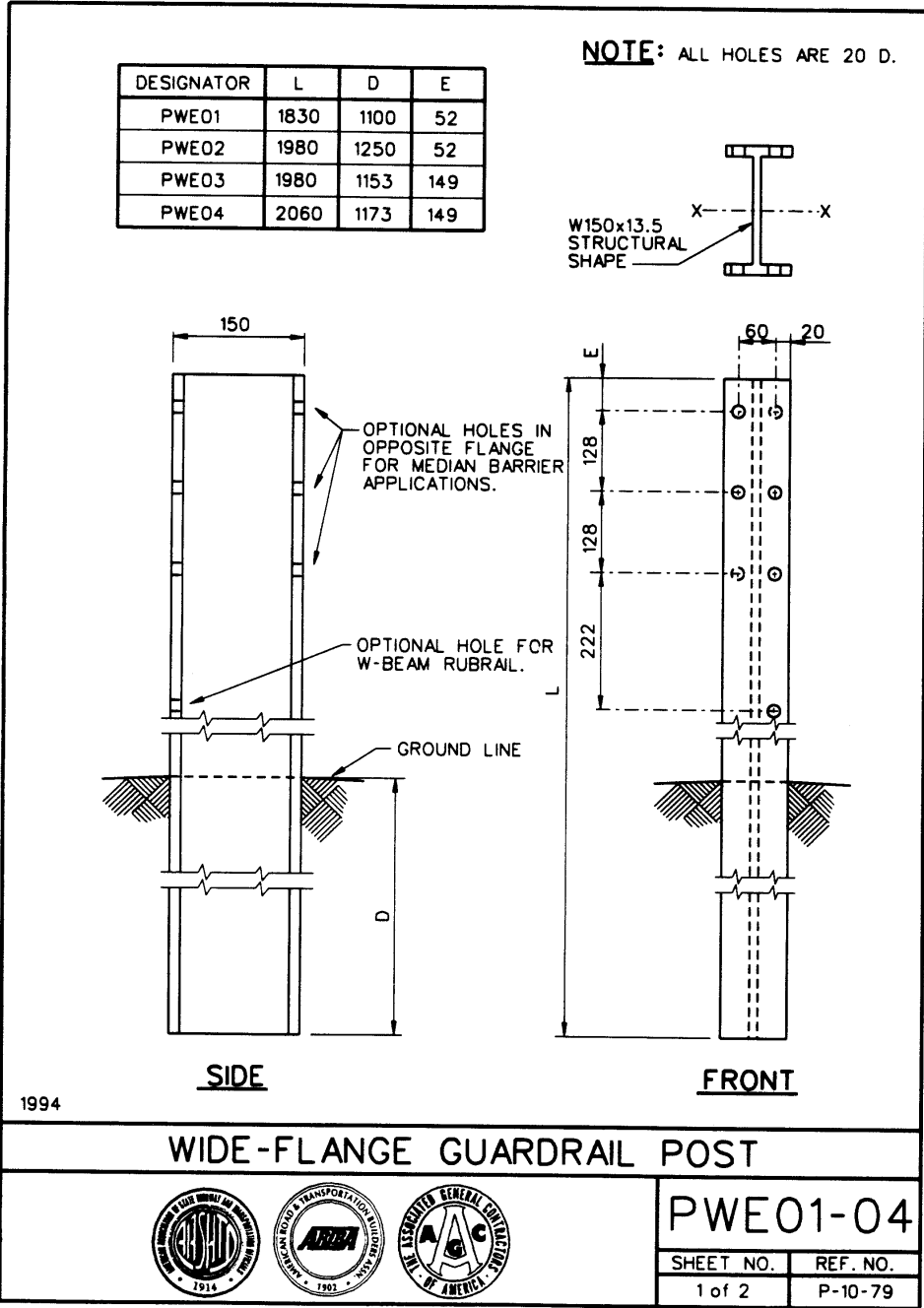
Figure 4.20: Drawing of the 150x13.5 steel guardrail post.*(59)*

122

Top View

101.6 mm

Front View   Side View

Groundline

1100 mm

1830 mm
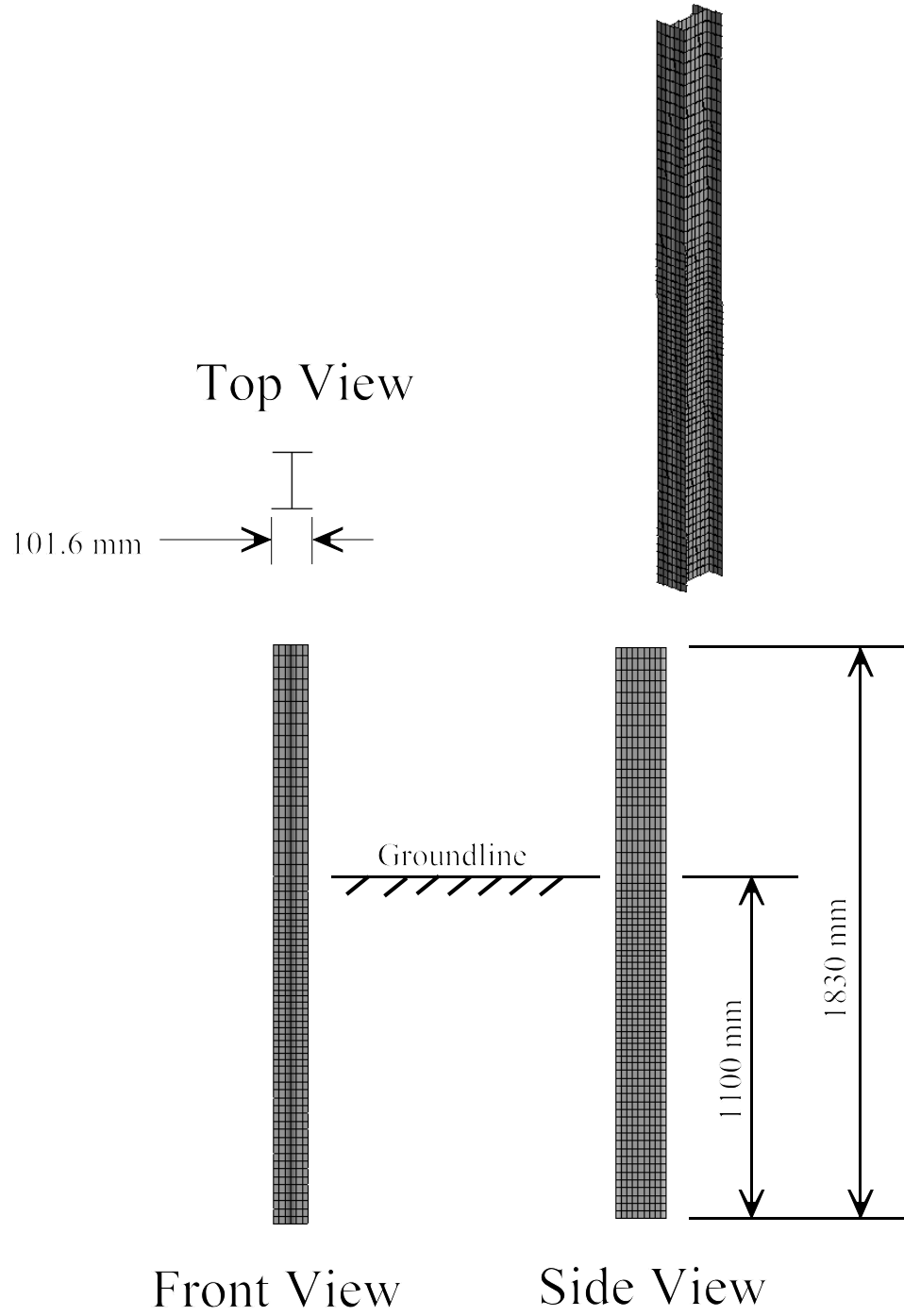
Figure 4.21:   Finite element model of guardrail post in impact region (fine mesh).

Top View

101.6 mm

Groundline

1100 mm

1830 mm

Front View   Side View
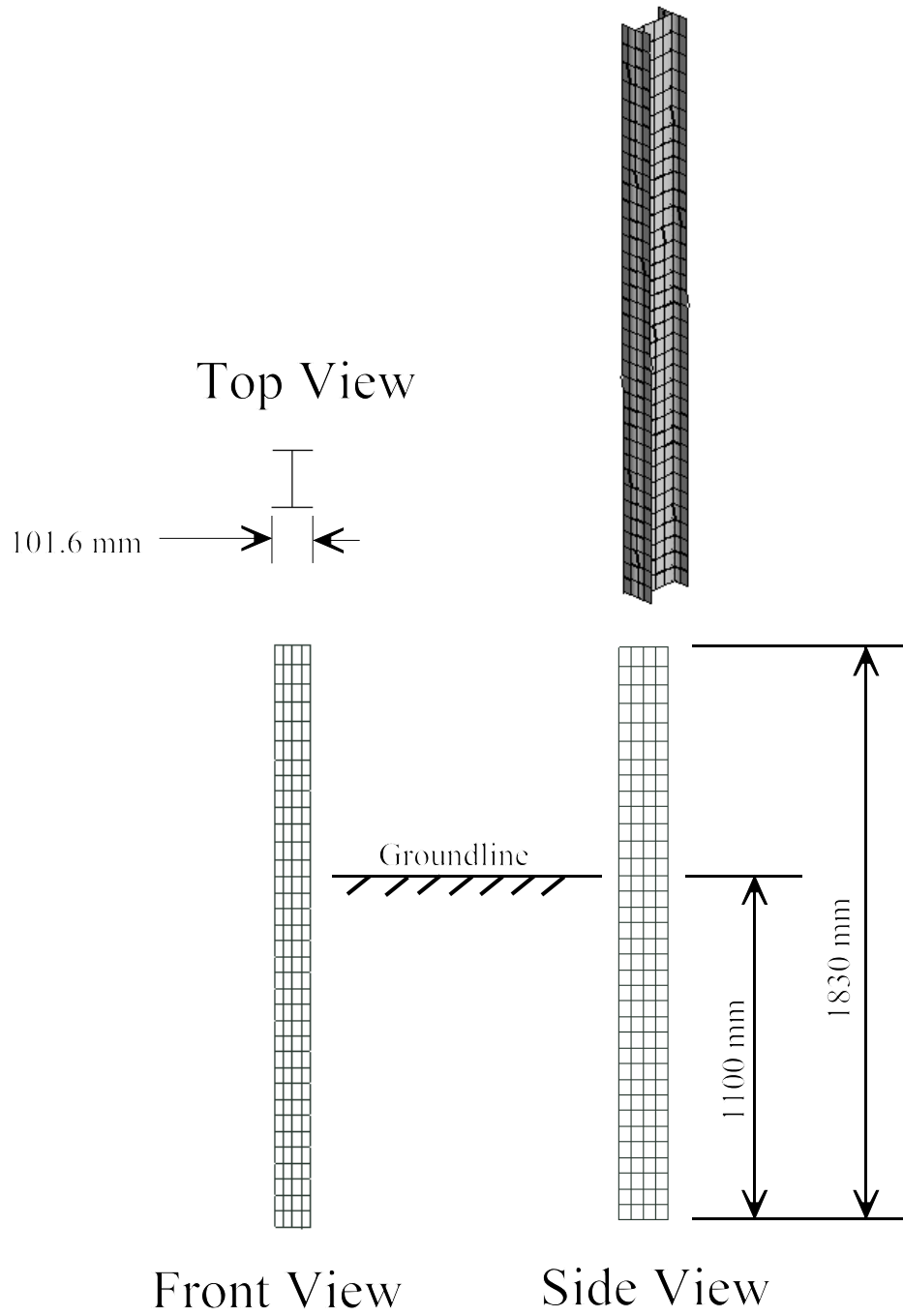
Figure 4.22: Finite element model of guardrail post in non-impact regions (coarse mesh).

Table 4.4: LS-DYNA material properties for modeling AASHTO M-183 steel using material type 24. *(60)*

Density (Mg/mm³)						7.86E-09
Young's Modulus (MPa)						200.0E+03
Poisson's Ratio						0.30
Yield Stress (MPa)						315.0
Strain Rate Effects			Cowper Simons model *(61)* with D = 100.4 p = 4.9			
Increments of Strain	0.0 0.019 0.625 1.00	0.050	0.165	0.330	0.495	
Increments of Stress (MPa)	315.0 315.0 507.0 507.0	428.0	501.0	504.0	507.0	

Mesh Sensitivity Study - To determine the proper mesh density the Belytschko-Lin-Tsay (BT) shell element with five integration points through the thickness was used, and the element size was reduced until convergence of the simulations were obtained. The mesh sensitivity analysis involved the PWE01 post model supported by non-linear springs representing soil interaction (see section 4.2.4 for details of soil modeling) and a displacement-time history was applied to the post at 550-mm above ground. The displacement-time history was obtained from a preliminary simulation of a full-scale impact event. The deformation of the post in the full-scale simulation was quite extreme and was considered a worse case scenario. The element size used for meshing the width of the flange and depth of the web of the coarse mesh post was 25 mm and 38 mm, respectively (see Figure 4.22). This results in four elements across the flange and four elements across the web. The mesh on the flange and web was refined in each simulation by adding one element until convergence was reached. Convergence was based on the

external work done in deforming the post (e.g., direct function of force) and the mode of deformation. The resulting mesh is shown in Figure 4.21, with six elements across the flange and nine element making up the web.

Element Formulation - The fine-mesh model of the post was used to investigate the proper element formulation for the post. Four different element types were used in the model:

     1) the Belytschko-Lin-Tsay (BT), type 2 in LS-DYNA,

     2) the Belytschko-Wong-Chiang, (BWC), type 10,

     3) the Hughes-Liu, (HL), type 1 and

     4) the Co-rotational Selectively Reduced Integration Hughes-Liu, (HLSR), type 7.

There was minimal difference in the results using each of these element types, however, the simulation using the BWC element did result in a less stiff response than the others. The analysis time for using each of the element types was significantly different, with the BT element being the most efficient. Table 4.5 lists the analysis time for each run and the analysis time for each run normalized with respect to the BT element simulation.

Based on these results the BT element was selected as the element type to be used for the posts in the modified G4(1S) model.

Table 4.5: Analysis time for the model using various element formulations.

Element Formulation	Analysis Time (minutes)	Analysis Time/BT Analysis
BT	19	1
BWC	21	1.1
HL	67	3.5
HLSRI	113	5.9

Through Thickness Integration Points - When a shell element is in pure tension or

compression the number of integration points is insignificant since the stress and strain

will be the same at all points through the thickness of the element. For elasto-plastic

bending of shell elements, however, the number of integration points through the

thickness of the shell is important where only a portion of the cross-section of the

element is plastically deformed. For the given stress profile shown schematically in

Figure 4.23, the use of only three integration points will result in the entire section

becoming plastic too early, the deflection will be relatively high and no elastic rebound

will occur. Using a higher number of integration points through the thickness will better

capture the stress profile through the thickness of the element, thus the computed

deflections will be much lower and significant elastic rebound will occur.

In the present case, the W150x13.5 posts of the guardrail bend during impact. The

flanges of the post are primarily in tension and compression on the front and back side of

Stress Profile   3 Int. Points   5 Int. Points
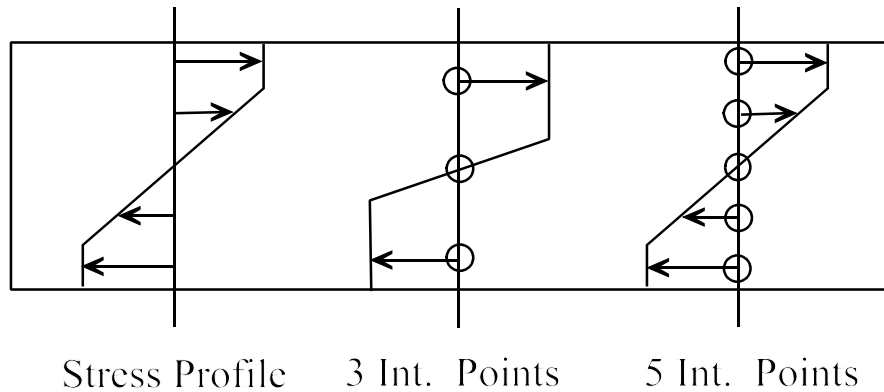
Figure 4.23:   Schematic of stress-profile through the thickness of a shell element using three- and five-integration points, respectively.

the post, respectively. Similarly, during impact the web of the post is in a state of tension or compression until either the web or the compression flange buckles. When buckling occurs the stress and strains will vary through the thickness in those localized areas of the buckle, but it has little effect on the overall stiffness of the post. This was confirmed by running the simulation discussed in the previous section with both three and five integration points through the thickness of the elements; the results were identical. Therefore, the element formulation that will be used to model the posts of the modified G4(1S) guardrail will be the Belytschko-Lin-Tsay (BT) shell element with three integration points through the thickness.

4.2.4 *Post and Soil Interaction*

The lateral stiffness of strong-post guardrails arises from the posts being driven into the soil, so the post-soil interaction may be regarded and analyzed as laterally loaded piles.

128

There are numerous modeling techniques for solving laterally loaded pile problems, although such techniques generally have been used for static conditions. In finite element analysis of such problems there are two basic approaches that are commonly employed:

- The continuum finite element approach in which the post is embedded in a soil continuum of solid finite elements, and

- The subgrade reaction approach in which the post is supported by an array of uncoupled springs.

Although both of these methods have advantages and disadvantages, the subgrade reaction approach is the most practical and computationally efficient approach for routine analysis. In a previous FHWA sponsored effort the subgrade reaction approach was utilized and a post-soil interaction model was developed which exhibited the type of behavior typically experienced during field tests.*(65)(66)* The force-deflection relationship is a non-linear function of the lateral post deflection, the depth below ground, the shape of the post, as well as the soil type and moisture content. This method yields satisfactory results if the post rotation is not so excessive that the vertical component of force becomes significant. This method has been used successfully in simulating the impact response of weak-post guardrails, strong post guardrails and guardrail terminals.*(47)(51)(64)(65)*

The soil-continuum modeling approach has also been employed in the study of post-soil

129

interaction for guardrail posts of the G4(1S) guardrail by Tabiei and Wu.*(67)* In their

study a model of the W150x13.5 post embedded in a soil continuum of solid finite

elements was developed. It was concluded that such a model would not be appropriate

for use in a full-scale model of the G4(1S) guardrail system, due to the immense

computational requirements of such an analysis. The post-soil model that they used in

the G4(1S) guardrail model consisted of the post supported by springs, similar to the

subgrade reaction method. The primary difference between their method and the

subgrade reaction method is that instead of using empirical equations they used the

results of the soil-continuum finite element model to characterize the stiffness properties

of the springs simulating soil resistance. It is to our knowledge, however, no material

model formulations in LS-DYNA that can accurately simulate soil behavior of guardrail

posts rotating in soil (*e.g.*, low confinement of soil and soil failure). It was also not

mentioned in their report how the soil-continuum model was validated.

The subgrade reaction method as described in Plaxico *et al*. was used in the current study

to simulate the post-soil interaction in the modified G4(1S) guardrail model.*(64)* An array

of non-linear springs was attached to the back flange of the posts to simulate soil

resistance in the lateral direction (with respect to the guardrail system). Similarly, an

array of springs was attached to the web of the post to simulate the soil resistance in the

longitudinal direction. The springs were connected to a line of nodes at 100-mm

increments of depth below grade, as shown in Figure 4.24. The force-deflection

characterization of the springs were computed based on the method described in Plaxico

130

et al., in which the spring stiffness increases with depth.*(64)* The soil-spring model is adequate for simulating both lateral and longitudinal deflections of the post (*i.e.*, with respect to the guardrail system), as well as, torsion of the post in soil.
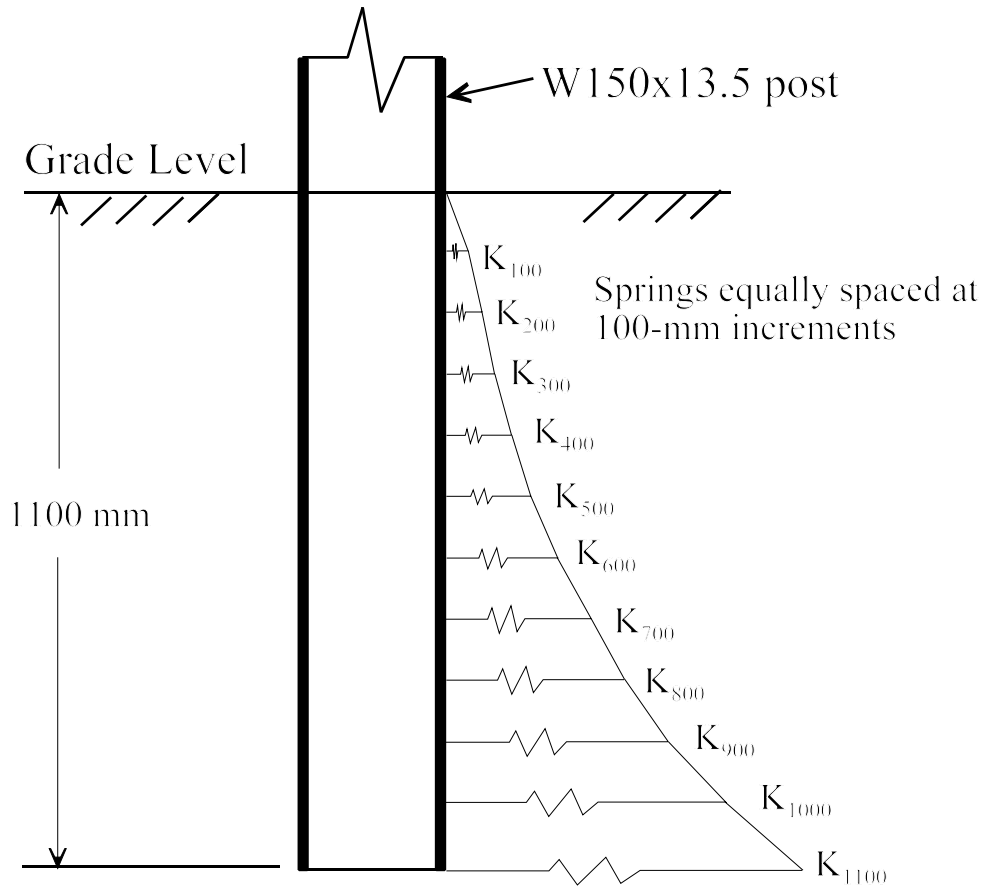

Figure 4.24: Schematic drawing of soil-springs attached to guardrail post below grade.

The post-soil model was validated with full-scale bogie impact tests of the W150x13.5 post embedded in soil that were conducted at the Midwest Roadside Safety Facility.*(68)*

The soil material in the tests conformed to AASHTO M 147-65 Gradation B (NCHRP Report 350 Strong Soil). The 946 kg MwRSF rigid nose bogie vehicle was used in the tests. The impact point on the posts was at 550-mm above grade and the impact direction was perpendicular to the flange of the post (*i.e.*, strong direction of post). There were a total of seventeen tests conducted in their study which involved both steel and wood posts, and four of these tests involved the W150x13.5 posts: WISC-1, WISC-2, WISC-3 and WISC-4. The variables in those four tests were the soil density and impact speed. The moisture content was relatively dry (3% - 7%) and was well below the optimum moisture content of 17 percent, with the exception of test WISC-2 which had a moisture content of 26 percent (*i.e.*, saturated conditions). The test matrix for these tests is shown in Table 4.6. In each of these tests the bogie was stopped by the posts. There was moderate rotation of the posts during impact, with slight deformation of the post flanges in tests WISC-3 and WISC-4.

Table 4.6: Test matrix for bogie impact tests of W150x13.5 posts embedded in soil*(67)*.

Test Number	Soil Density (kg/m³)	Moisture Content	Impact Velocity (m/s)
WISC-1	1980	DRY	4.6
WISC-2	2018	26 %	6.0
WISC-3	2110	DRY	5.4
WISC-4	2240	DRY	5.9

The W150x13.5 post and soil-spring finite element model was used to simulate three of

these tests: WISC-1, WISC-3 and WISC-4. A finite element model of the impact head of

the MwRSF bogie vehicle was developed with the correct geometry of the impact head,

as shown in Figure 4.25. The mass of the bogie model was 946 kg, consistent with the

mass of the test vehicle. The soil

properties corresponding to each of

the tests were input into the soil-

spring model (note: the soil-springs

are not shown on the model in

Figure 4.25). The results from the

simulation and tests are shown in

Figures 4.26, 4.27 and 4.28, which

show the force versus displacement

at the impact location of the posts

Figure 4.29 shows the deformation

of the finite element model for

simulations of tests WISC-1,

WISC-3 and WISC-4.
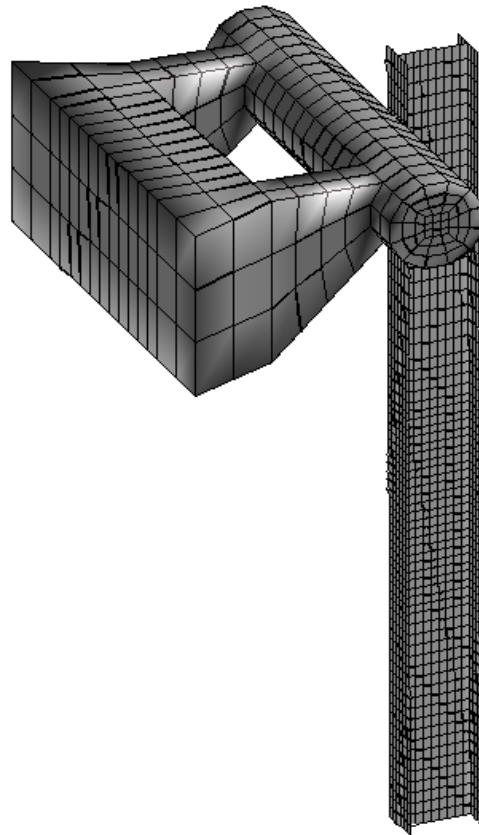
Figure 4. 25: Finite element model used for post-
soil model validation.

The peak load values in the tests are much higher than those obtained in the

corresponding simulations. The peak force values in the tests occur during the initial

loading phase on the posts and are due to the inertia of the soil which does not exist in the

finite element model. The average force in the simulations, however, are similar to those

133

Plot 2: Force Versus Deflection At Impact Location
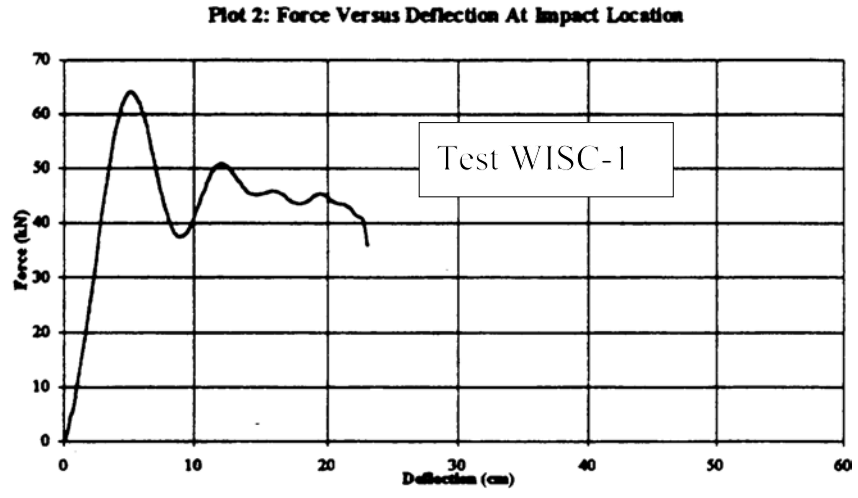
(a)
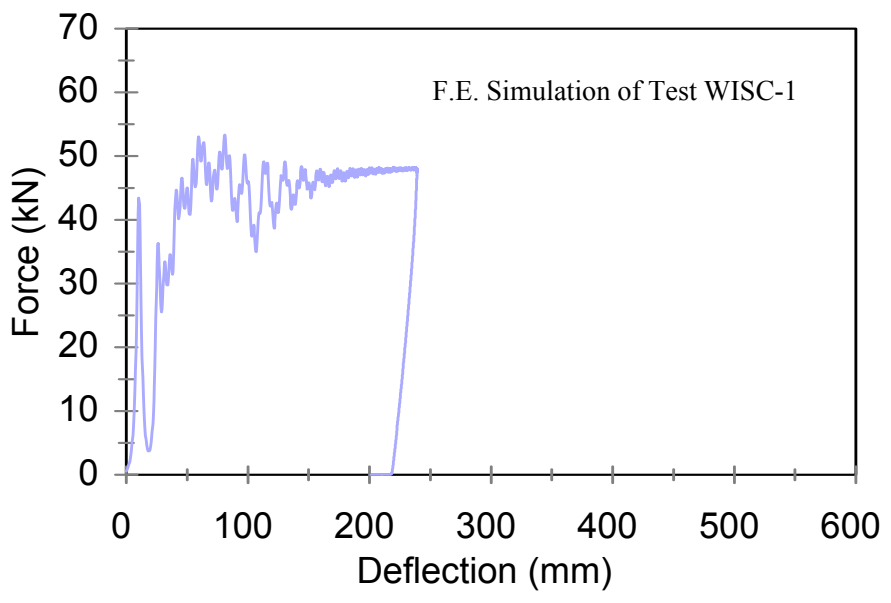
(b)

Figure 4.26: Results of (a) test WISC-1*(67)* and (b) finite element simulation.

Plot 2: Force Versus Deflection At Impact Location

Test WISC-3

(a)

F.E. Simulation of Test WISC-3
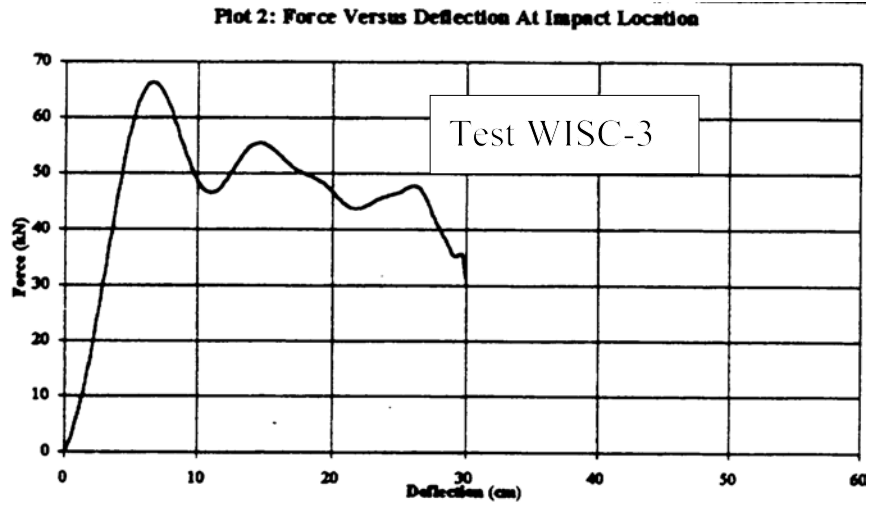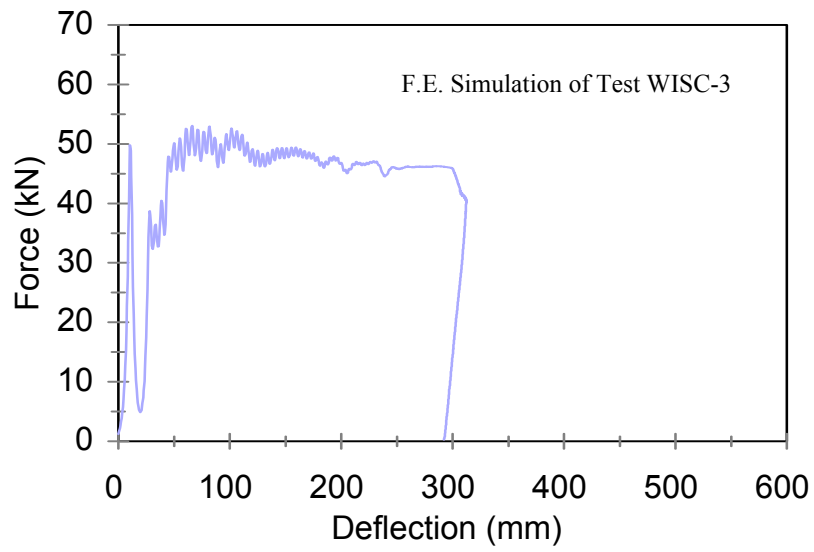
(b)

**Figure 4.27**: Results of (a) test WISC-3*(67)* and (b) finite element simulation.

Plot 2: Force Versus Deflection At Impact Location

Test WISC-4

(a)

F.E. Simulation of Test WISC-4
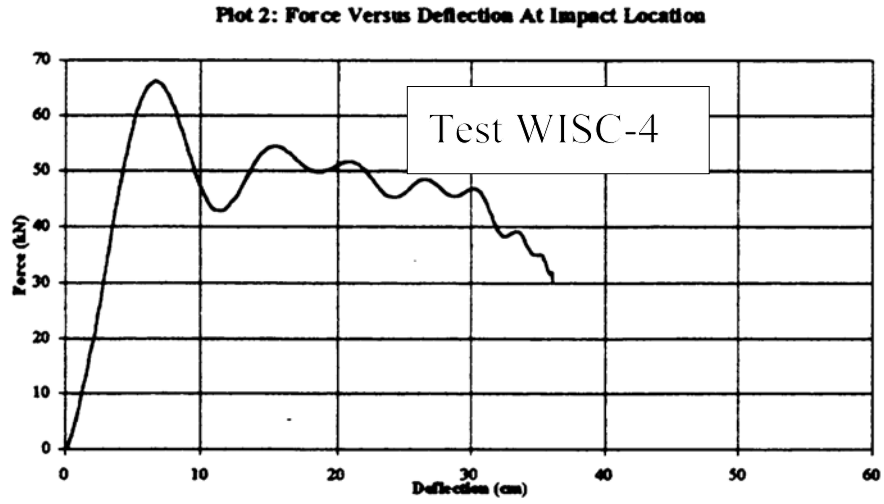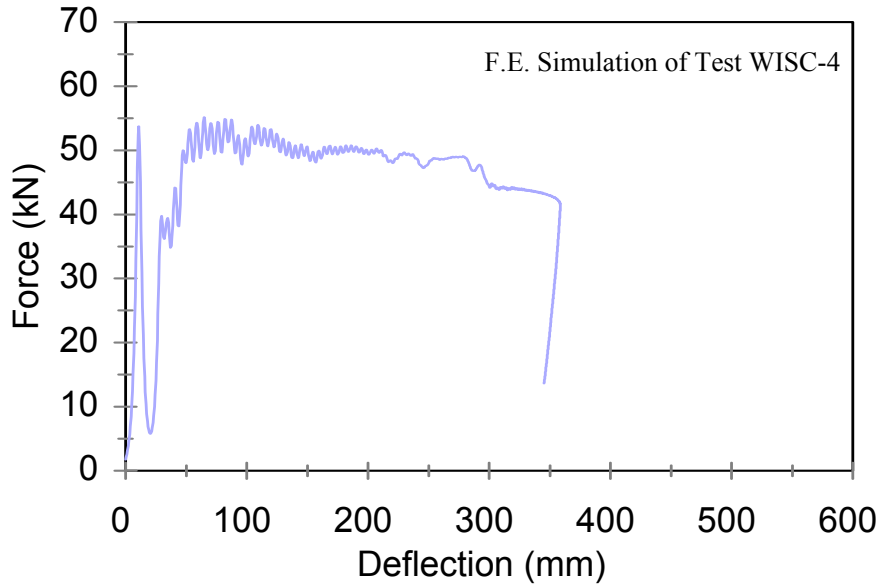
(b)

Figure 4.28:   Results of (a) test WISC-4*(67)* and (b) finite element simulation.

WISC-1	WISC-3	WISC-4
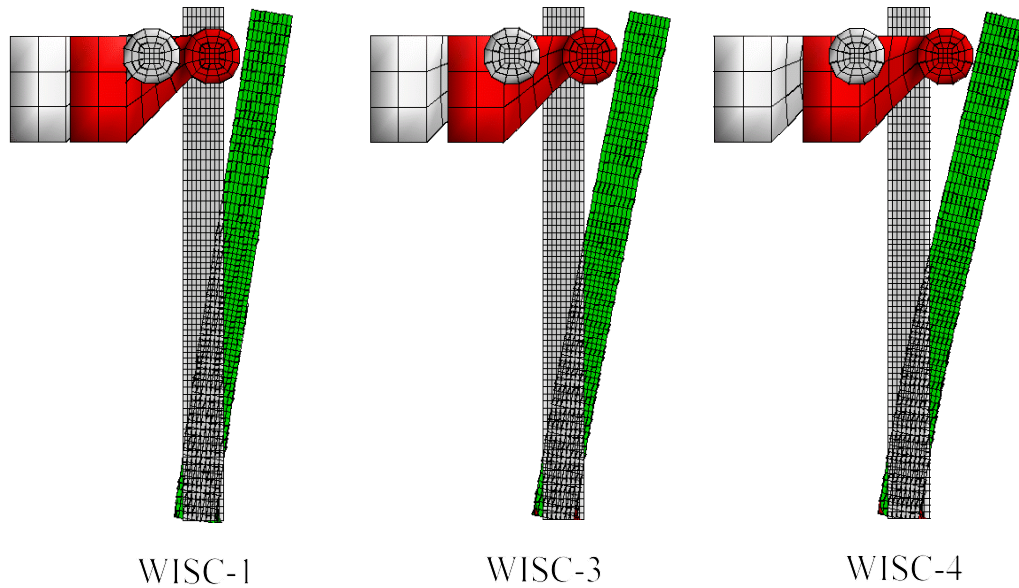
Figure 4.29: Results of finite element simulation of post-soil tests.

of the tests. Correspondingly, the total displacement of the post and the energy absorbed by the post and the soil during impact is similar in the tests and simulations as well. A summary of test and simulation results is shown in table 4.7.

Table 4.7: Summary of test and simulation results for post-soil study.

	Impact Velocity (m/s)		Max. Deflection (mm)		Average Force (kN)	
Test No.	Test	Simulation	Test	Simulation	Test	Simulation
WISC-1	4.6	4.6	234	249	42.8	40.2
WISC-3	5.4	5.4	314	306	43.9	45.1
WISC-4	5.9	5.9	348	342	47.3	48.1

4.2.5   W-Beam Rail to Post Connections

In both the G4(2W) and the modified G4(1S) strong post guardrail systems, the w-beam rail is fastened to the post with a 16-mm diameter bolt that is 203 mm long and passes through a wood blockout and is fastened to the back side of the guardrail post with a hex-nut, as shown in Figure 4.3.*(59)* The bolted connection is typically located on the up-stream flange of the post in the G4(1S) guardrail systems. During a collision these bolted connections experience high loads in the impact region of the guardrail, and as a result the head of the bolt is pulled through the slotted hole in the w-beam, thereby, releasing the w-beam from the post, as shown in Figure 4.30.*(32)(57)* The behavior of these connections can have a significant effect on the performance of the guardrail system. For example, if the connections are too strong, the w-beam is likely to be pulled to the ground with the post and result in the vehicle overriding the guardrail. If the connections are too weak, the rail can pull away from the post too soon allowing the rail to drop and the vehicle to penetrate behind the system.

Before Impact   After Impact
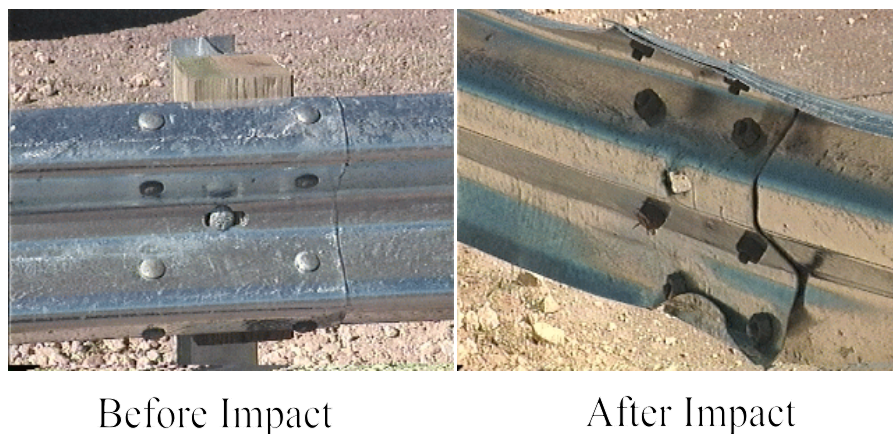
Figure 4.30:   Bolted connection of w-beam-to-post before and after
              impact.*(57)*

138

The problems associated with simulating the bolted connection of the w-beam to the post in the finite element model are similar to those discussed previously for simulating the splice connection. One major difference, however, is that the w-beam rail connection must be able to simulate failure. There are a few options for modeling the connection:

1. model the connection in geometric detail by explicitly modeling the bolt and the slotted hole in the w-beam,

2. use the nodal-rigid-body-spotweld option in LS-DYNA to connect the w-beam to the blockout with a failure condition based on strain or force, or

3. use nonlinear springs with a force-displacement relationship that accurately characterizes the behavior of the connection.

The first option could be very computationally demanding depending on the element size used in the model. Either of the remaining two methods could be used effectively, provided the necessary parameters for them are specified. The nodal-rigid-body-spotweld option entails a rigid beam element connected to one node on the w-beam and one node on the blockout at the bolt location. This method does not allow separation of the nodes in the connection until the strain in the material surrounding the spotweld reaches a specified failure value or until the force in the spotweld reaches a critical magnitude. In previous studies, the connection was modeled using the spotweld option with the failure of the spotwelds based on a relatively low axial force failure criteria with an infinitely large shear force failure criteria.*(47)* The idea being that the connections

will not fail up-stream or down-stream of the impact region where the forces in the connections are predominately in pure shear, but, in the impact zone where the connection is in tension, the spotwelds are defined to fail relatively easily, simulating the head of the bolt pulling through the w-beam slot during impact.

Tabiei and Wu used the third option, a non-linear spring, to simulate the behavior of the connection.*(66)* The force-displacement relationship of the spring in their model was obtained from a detailed finite element model of the connection. Two scenarios were used in the detailed model to determine the behavior of the connection. In the first case, the bolt was in the center of the slot in the w-beam and, in the second case, the bolt was placed at the edge of the slot. The forces generated in the connection during their analyses were obtained from the contact forces computed by LS-DYNA. The maximum forces required to pull the bolt-head through the slot of the w-beam in their simulations was 30 kN and 80 kN for the first and second case, respectively. They obtained the force-deflection characteristics of the connection in the finite element model and used them to define the properties of the nonlinear springs that were used to simulate the post-to-w-beam connection in the full model of the guardrail system. This method provides a reasonable approximation of the connection behavior. Their detailed model of the connection, however, only included one layer of w-beam; whereas the connection of the w-beam to the posts at splice locations where the bolt-head must pull through two layers of w-beam will have a much different response. In addition, the results were not validated with any physical experiments.

Laboratory Tests - A series of quasi-static laboratory tests of the w-beam/bolt connection were conducted in which the bolt head was pulled through the slot of the w-beam rail using the 1,780 kN Tinus Olsen axial load testing machine shown in Figure 4.31. The purpose of these tests was to isolate the failure mechanism of the bolted connection in order to provide data for validation of a finite element model of the connection. Four scenarios were investigated which are illustrated in Figure 4.32:

Case 1.   One layer of w-beam with the bolt positioned in the center of the slot in the w-beam,

Case 2.   One layer of w-beam with the bolt positioned at the edge of the slot in the w-beam,

Case 3.   Two layers of w-beams (e.g., a splice connection at a post) with the bolt positioned at the center of the slots in the both sections, and

Case 4.   Two layers of w-beams with the bolt positioned at the edge of the slots in both sections.

The test fixture and a test specimen are shown in Figure 4.31. The bottom right photo in Figure 4.31 shows the underneath surface of the lower cross-head of the Tinus Olsen machine where a 102x115 mm rectangular opening exists. A steel rod with a diameter of 28 mm was clamped in the upper cross-head of the test machine, and the rod extended through the lower cross-head. A nut from a post-bolt was welded to the end of the steel rod, and the w-beam specimens were fastened to the rod with a post-bolt. The end of the steel rod and nut assembly is visible in the bottom photo of Figure 4.31.

141
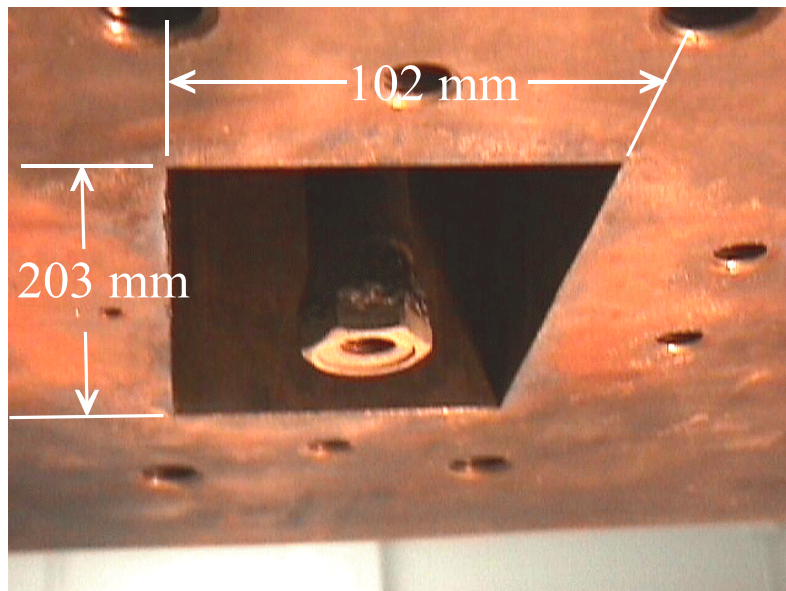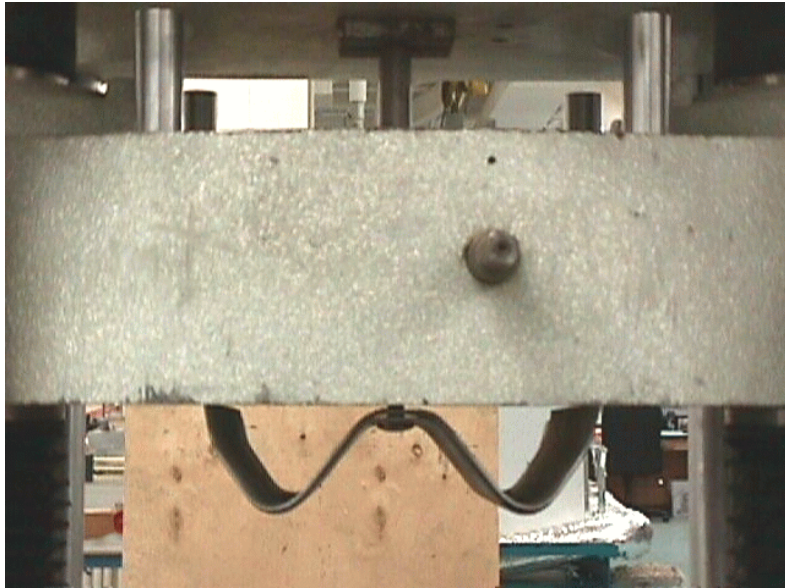
Figure 4.31:   Test fixture and specimen used in w-beam/bolt
connection tests.
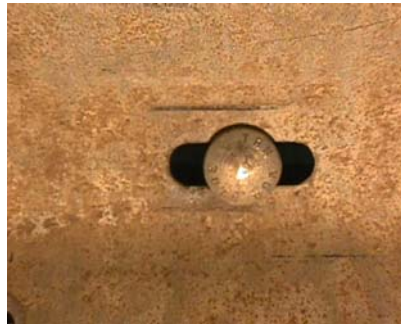
Setup 1   Setup 2
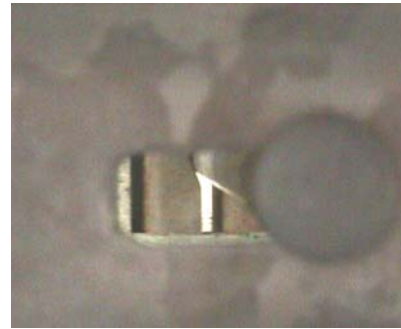
Setup 3   Setup 4

Figure 4.32:   Four load case scenarios investigated in laboratory tests.

During loading, the bolt-and-nut was pulled upward by the test machine at a constant displacement rate of 25.4 mm/minute. The w-beam was compressed against the surface of the lower cross-head, where the 102x115 mm opening in the cross-head ensured that the load was isolated to the immediate vicinity of the bolted connection.

Two tests were conducted for each of the four test cases. The results of the tests are

shown in Figure 4.33 and are summarized in Table 4.8. In each of the eight tests, the

failure mechanism of the connection was consistent; the head of the bolt was pulled

through the slot in the w-beam deforming the region of w-beam material surrounding the

slot, as shown in Figure 4.34. The displacement shown in Figure 4.33 is the displacement

of the bolt during loading that was measured using a string-pot displacement transducer.

The minimum pull-through force required to fail the connection occurred in case 1 (i.e.,

one layer of w-beam with the bolt in the center of the slot) with an average load of 18 kN.

The maximum pull-through force occurred in case 4 (i.e., two layers of w-beams with the

bolt positioned at the corner of the slot) with an average load of 64.7 kN.
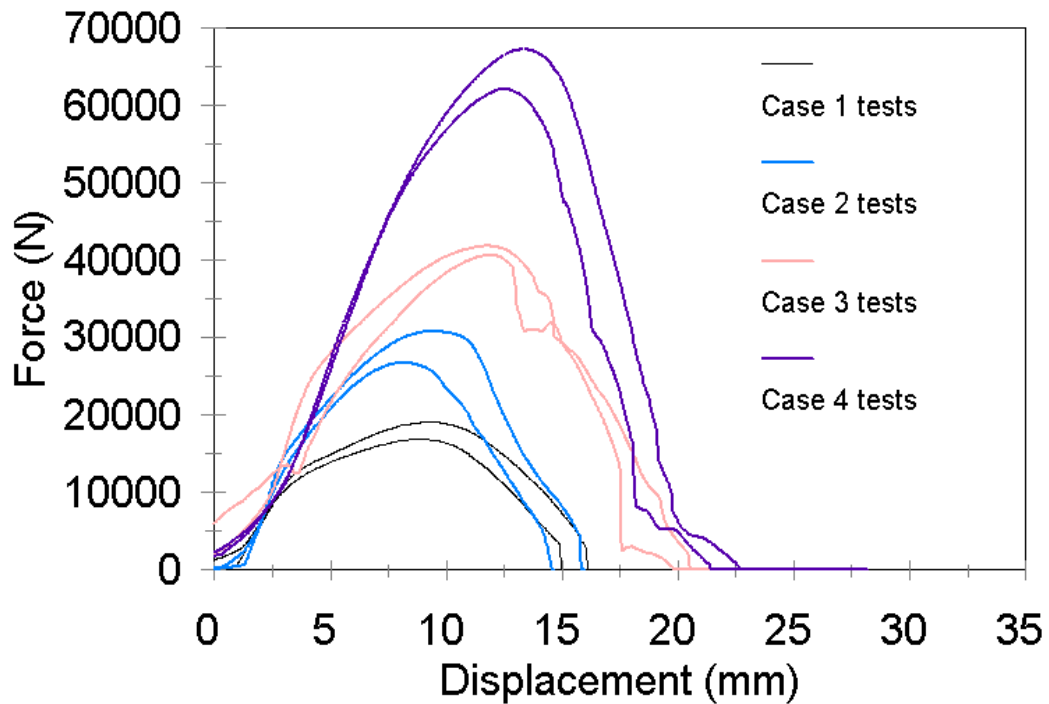
Figure 4.33: Force-deflection results from uniaxial load tests on bolted
connection.

Table 4.8: Summary of post-bolt connection failure from laboratory tests.

Test Case	Maximum Force (kN)		
	Test 1	Test 2	Average Test Max.
Case 1	16.8	19.1	18.0
Case 2	26.7	30.7	28.7
Case 3	40.6	41.1	41.0
Case 4	62.1	67.3	64.7

Load case 1   Load case 2

Load case 3   Load case 4

Figure 4.34:   Deformed w-beam slots after failure of the bolted connection in
each of the load cases.

Finite Element Model - Two of the three modeling techniques listed previously were considered for modeling the connection of the w-beam to the posts and blockouts: the *nonlinear springs* option and the *geometric detail* option. The response of the connection using the nonlinear springs is not sensitive to element size, thus the connection would be modeled the same for each connection regardless of the mesh density at each connection throughout the model. The connections were modeled using nonlinear springs primarily because of the extensive computational time requirements needed to conduct an analysis with connections modeled in geometric detail. The detailed models that were developed were, however, considered more accurate for modeling the connection.*(69)* The details of that effort are summarized below.

Summary of Detailed Connection Model Results - Three finite element models of the connection were developed, each with a different mesh density in order to determine the necessary mesh refinement such that reasonable results were obtained from the finite element model. The three finite element meshes are shown in Figure 4.35. A load was applied to the simulated bolted connection in the same manner as was done in the tests. An additional model was developed that adopted the mesh of model 3 with a modified thickness of the w-beam material such that an "equivalent" stiffness was achieved. The w-beam was modeled using a piecewise linear elastic-plastic material law with strain hardening (*i.e.*, material type 24 in LS-DYNA). The material properties for the w-beam were consistent with those provided by Wright and Ray.*(60)* Each of the models are briefly described below. The results of the simulations of models 1, 2 and 4 are

146

compared to the test results in Figures 4.36 and 4.37 and in Table 4.9.

Model 1.   Detailed geometric model of connection with a dense mesh (e.g., element

size of 1.4x2.4 mm),

Model 2.   Detailed geometric model of connection with a medium density mesh

(e.g., element size of 2.9x2.5 mm), and

Model 3.   Detailed geometric model of connection with a relatively coarse mesh

(e.g., element size of 5.6x7.9 mm).

Model 4.   Coarse mesh model (e.g., element size of 5.6x7.9 mm) with modified

thickness.

The smallest element dimension (of the deformable elements) in each the three models

was 1.4 mm, 2.9 mm and 5.6 mm, respectively, and those elements were located around

the edge of the slotted hole in the w-beam. Model 1, with an element size of 1.4 mm,

accurately replicated the laboratory test results in all four test case scenarios. Model 2,

with an element size of 2.9 mm, also provided reasonable results, however, the element

type used in the w-beam mesh of model 2 was changed to the fast-fully-integrated

element formulation in LS-DYNA (i.e., element type 16) in order to eliminate the zero

energy modes. The results obtained from Model 3, with an element size of 5.6 mm,

demonstrated a much higher failure load than was observed in the tests. The coarse mesh

of Model 3 was also very susceptible to zero energy modes.
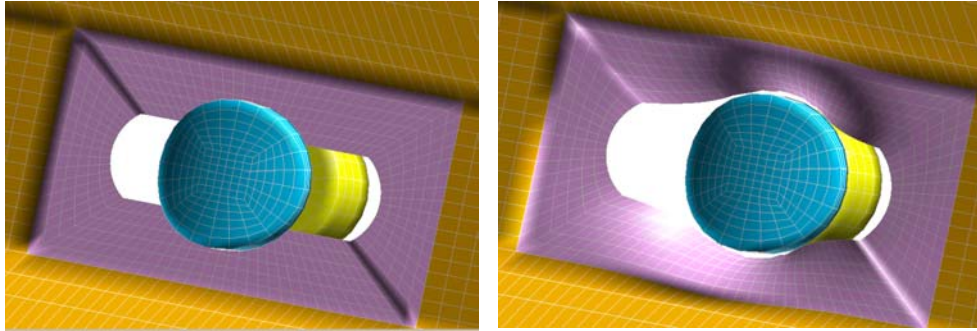
Model 1 - fine mesh model
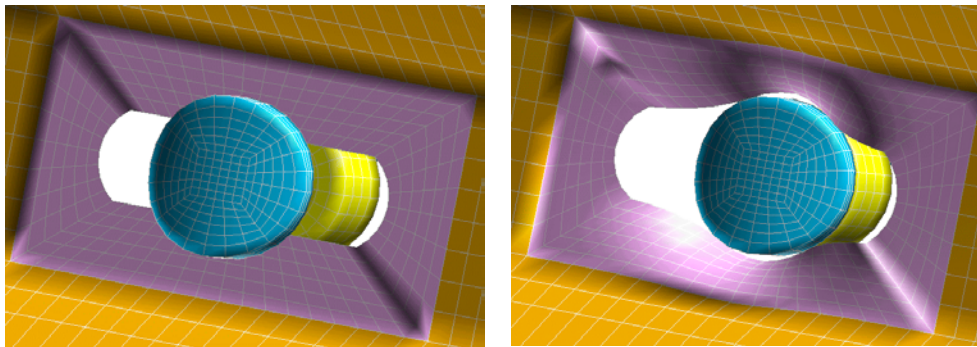
Model 2 - medium mesh model
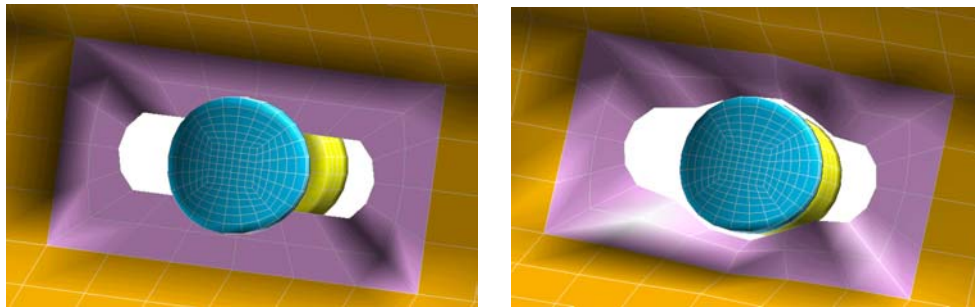
Model 3 - coarse mesh model

Figure 4.35:   The finite element mesh of the bolted connection in each of the three finite element models.
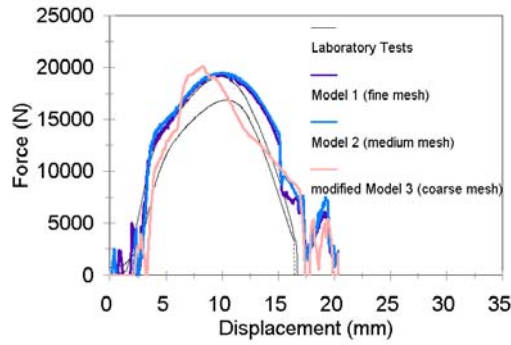
Load Case 1
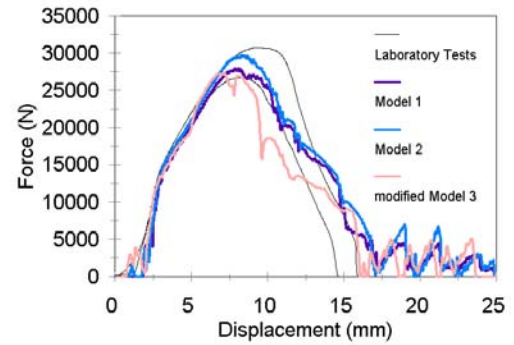
Load Case 2
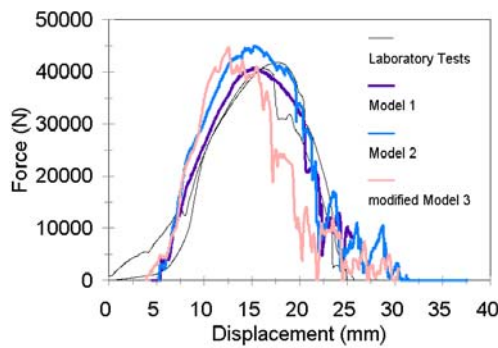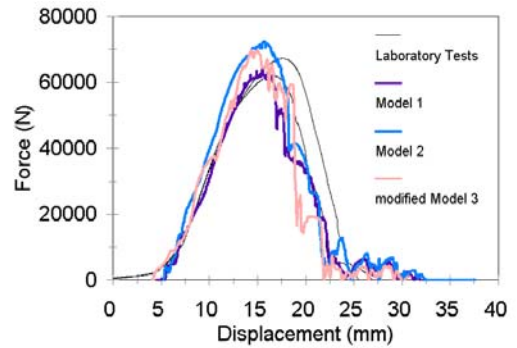
Load Case 3

Load Case 4

Figure 4.36: Force-deflection results from F.E. model 1, F.E. model 2 and modified F.E. model 3 compared to test data.
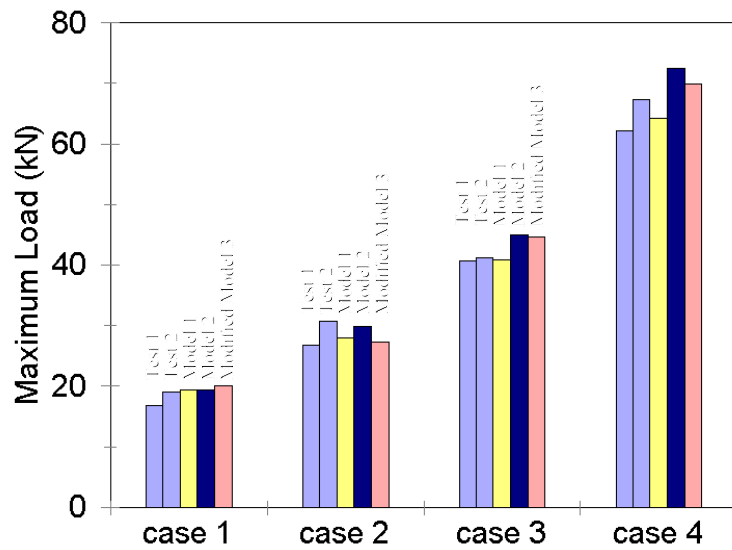

Figure 4.37: Maximum force required to fail bolted connection in tests and simulations.

149

Table 4.9: Summary of post-bolt connection failure from tests and simulation.

Test Case	Maximum Force (kN)				
	Test 1	Test 2	Model 1 (fine mesh)	Model 2 (med. Mesh)	Modified Model 3 (coarse mesh)
Case 1	16.8	19.1	19.4	19.5	20.1
Case 2	26.7	30.7	28.0	29.8	27.3
Case 3	40.6	41.1	40.8	45.0	44.7
Case 4	62.1	67.3	64.2	72.4	69.8

Models 1 and 2 are considered impractical for use in routine analyses of a complete

model of a guardrail system due to the small time-step required to perform an explicit

finite element analysis with those models. The coarse mesh of model 3, on the other

hand, required very little computation time to complete the analysis but was considered

inadequate because of its overly stiff response. In order to obtain a model of the

connection that was both computationally efficient and which also produced reasonable

results, the thickness properties of the w-beam material in the region of the slotted hole in

model 3 were modified such that an "equivalent" stiffness of the connection was

achieved. This modification resulted in a finite element model of the connection that

could be used effectively in a complete model of a guardrail system.

4.2.6 *Boundary Conditions Simulating Guardrail Anchor System*

The total installation length of guardrail systems including standard end terminals is

around 53 m for crash test installations.*(57)* A finite element model of a complete

guardrail system would require extensive computational resources and would be

impractical for use in routine analyses. To make the model efficient for analysis, only a

portion of the guardrail was modeled. The unmodeled portion of the guardrail was

simulated by applying boundary conditions to the ends of the w-beam rail using simple

modeling techniques. The boundary conditions must, however, result in realistic behavior

of the guardrail ends and anchor systems.

The entire guardrail and its anchor systems are affected during an impact event and each

component of the system has some significance in the performance of the guardrail. In

weak-post guardrails all the load in the w-beam rail is carried by the anchor systems,

while the posts serve only to keep the rail at the proper height during impact. In strong

post guardrails, such as the G4(2W) and the G4(1S), much of the redirection of the

vehicle is provided by the guardrail posts (in the local area of the impact) rotating in soil

and, thus, a smaller proportion of the load is transferred to the anchors.

In finite element models of the G4(2W) guardrail developed by Plaxico *et al.*, the

boundary conditions on the ends of the rail were modeled using linear spring

elements.*(47)* The stiffness of the springs were defined using the relationship, $K = EA/L$,

where K is the stiffness of the spring, E is the modulus of elasticity of steel, A is the

cross-sectional area of the w-beam and L is the length of the unmodeled portion of the

guardrail. This approximation simulates the unmodeled portion of the guardrail as a

continuous element with a fixed condition on the end and does not include the effects of anchor movement nor "slip" displacement in the rail splice during impact. The use of the linear spring elements was justified in their model based on results from previous crash tests of the standard G4(2W) guardrail, in which no movement of the anchor system was observed. Their model was validated through both qualitative and quantitative comparisons of the simulated results to those of actual crash tests.(37)*(47)*

In previous full-scale crash tests involving G4(1S) and the modified G4(1S) guardrails, however, the tensile loads in the w-beam were sufficient to cause substantial movement of the anchors. Thus, the use of linear spring elements to simulate the boundary conditions in such a model is not applicable.*(57)(59)* There was not enough information provided in the crash test reports to determine the relationship between rail tension and deflection of the anchor systems. A literature search was conducted to find information about the force-deflection characteristics of guardrail anchor systems due to tension in the rail. Only one reference was found, but it could not be obtained. The paper title was "Static Test of an Indiana Standard Guardrail." The study was sponsored by the Federal Highway Administration (FHWA) and was conducted by Indiana State Highway Commission Research and Training Center. The study entailed static tests in which a common guardrail end treatment was installed and a tensile load was applied to the system in line with the w-beam rail.

Since no other information was available, the response of a guardrail anchor system was

investigated using a submodel of the terminal section. The finite element model of the

Modified Eccentric Loader Terminal (MELT) that was developed by Patzner *et al.* was

used to develop a force-displacement relationship for the rail-end springs.*(66)* The

MELT model was converted to a straight anchor, and a displacement-time history was

applied to the finite element nodes on the end of the w-beam rail to generate a tensile

force in the w-beam, as shown in Figure 4.38. The resulting deformation of the anchor

model is shown in Figure 4.39 and the force-displacement response during loading is

shown in Figure 4.40. Although the model was not validated for this particular loading

case, the values obtained from the model were used to develop the force-displacement

properties for the non-linear springs that may be used as boundary conditions in the

modified G4(1S) guardrail model.
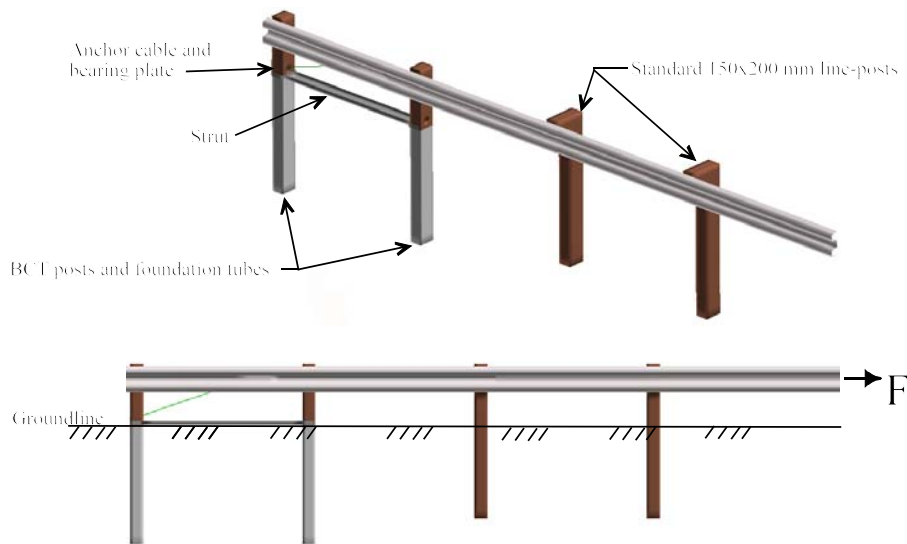
**Figure 4.38**: Finite element model of anchor system.
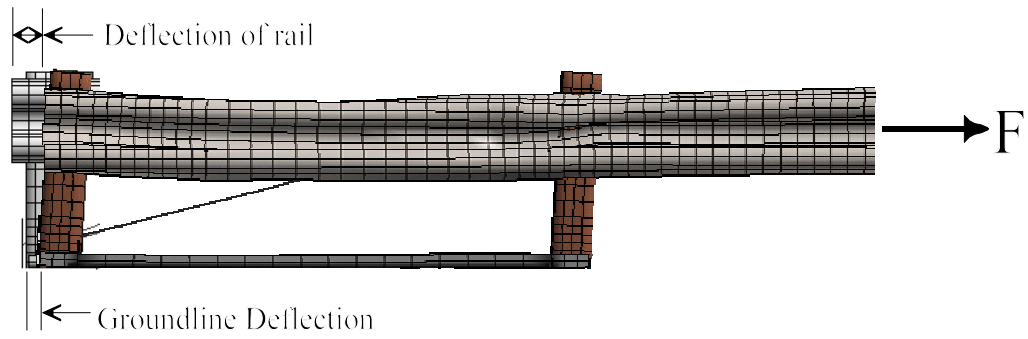
Figure 4.39: Deflection of BCT model due to tensile force F in submodel simulation.
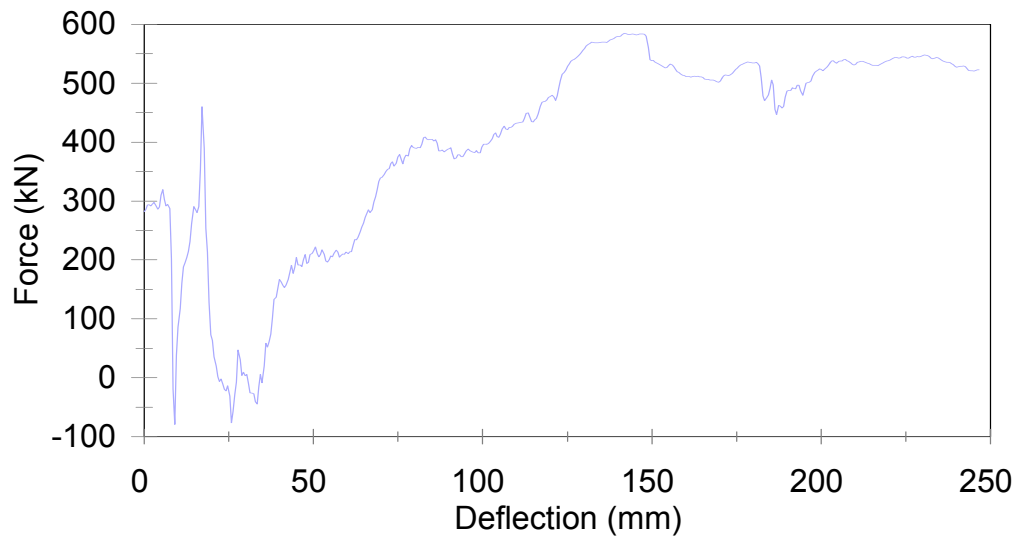

Figure 4.40: Force-deflection response of anchor model.

Another alternative is to model the terminal explicitly in the G4(1S) guardrail model. This of coarse will increase computation time but may be necessary to ensure accuracy when inertial effects due to the mass of the terminal components (*e.g.*, w-beam, posts, etc.) are important to the response of the system. For the purposes of this study it was decided that the response of the upstream guardrail terminal would have a significant effect on the response of the system and as such the terminal was modeled explicitly. The down stream terminal was modeled by using nonlinear springs as boundary conditions on the end of the w-beam rail as previously discussed.

4.3   Finite Element Model of a Chevrolet 2500 Pickup Truck

A finite element model of the Chevrolet 2500 pickup truck will be used in this research to simulate impact into various curbs and curb-barrier systems. The National Crash Analysis Center (NCAC) developed two models of the pickup truck that are available for use by the public: a reduced element model (C2500R) and a more detailed version (C2500D). The reduced model will be used in this study for reasons cited in Chapter 3. Although the suspension components in the NCAC C2500R model were crudely modeled and do not provide accurate response, this model has been used extensively by the researchers at WPI in previous studies for simulating vehicle-to-guardrail impacts and the performance of the model in those studies were satisfactory. In the current study, which involves the vehicle traversing curbs, the response of the suspension system plays a significant role in the impact event, thus the suspension model components must be carefully evaluated and validated with physical tests in order to have confidence in the

simulated results.

In an earlier phase of NCHRP Project 22-17 (i.e., the sponsor of this research) researchers at Worcester Polytechnic Institute modified the suspension components of the NCAC C2500R model.*(70)(71)* In their study a component test program was conducted to obtain accurate properties and characteristics of various suspension components. These modifications resulted in marked improvement in the response of the vehicle's dynamic behavior during impact with curbs. A summary of modifications and the extent of verification of each component model is given below in Table 4.10.

4.4   Validation of the Modified G4(1S) Guardrail Model

A finite element model of the modified G4(1S) guardrail with wood blockouts was developed using the previously discussed methodology, and is being used to simulate a full-scale crash test event. A full-scale crash test was conducted at TTI on November 16, 1995 (*i.e.*, TTI test 405421-1) which involved the modified G4(1S) tested under NCHRP Report 350 Test 3-11 impact conditions.*(57)* The test installation consisted of a 30.5 m long section of the modified G4(1S) W-beam guardrail system with a 11.4 m long Modified Eccentric Loader Terminal (MELT) terminal at each end. The total installation length was 53.3 m. The 2000P vehicle used in the test was a 1989 Chevrolet 2500 pickup truck. The test vehicle hit the rail just upstream of post 12 at a speed of 101.5 km/hr at an angle of 25.5 degrees. The guardrail successfully contained and redirected the vehicle. This crash test was used to validate the finite element model.

Table 4.10: Summary of modifications made to the NCAC C2500R pickup truck by Worcester Polytechnic Institute.

Component	Verification Summary
Front suspension coil springs	Properties verified with physical test data
Front suspension dampers	Properties verified with physical test data obtained from external source
Bump stops on front A-arms	Response verified through visual observation of computer model results and judgement.
Stabilizer bar	Response verified through visual observation of computer model results and judgement.
Rear suspension leaf spring	Spring properties for vertical stiffness verified with physical test data. Lateral and torsional stiffness properties obtained analytically.
Steering system properties	Properties verified through crude physical tests.
Steer stops on steering system	Response verified through visual observation of computer model results and judgement.
Tire model and properties	Response verified through visual observation of computer model results and judgement.
A-arm and rim models	Made rigid. Response verified through visual observation of computer model results and judgement.
Inertial Properties	Properties verified through data obtained from NHTSA and the Texas Transportation Institute.

In the finite element analysis, 34.6 m of the modified G4(1S) guardrail was modeled and

a simulated impact on the system was conducted using LS-DYNA. The NCAC C2500

version 9 model with suspension modifications made by WPI was used in the analysis to
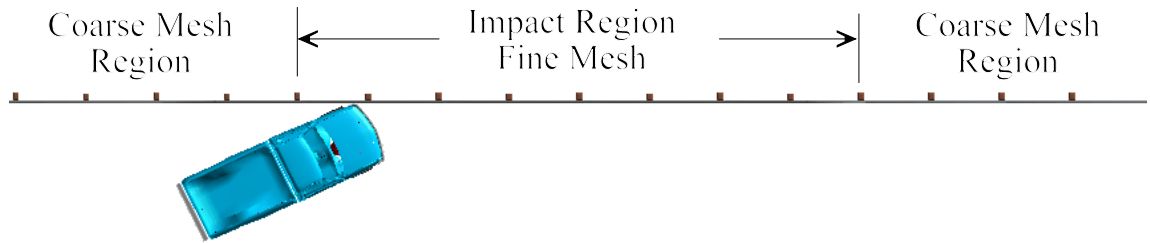
Figure 4.41:   Finite element model used in preliminary validation of G4(1S) guardrail model.

simulate the test vehicle. The finite element model is shown in Figure 4.5 and Figure

4.41.

This model uses nonlinear springs to simulate the splice connection, nonlinear springs to

simulate w-beam to post connection and nonlinear springs as boundary conditions

simulating the downstream anchor system. The upstream anchor system (i.e., MELT) was

modeled explicitly. The complete model of the guardrail system includes 79,577 nodes,

15,788 brick elements, 19 beam elements, 48,523 shell elements, and 7,647 discrete

spring and damper elements. The pickup model includes 17,650 nodes, 546 brick

elements, 30 beam elements, 15,960 shell elements, and 20 discrete spring and damper

elements.

The impact conditions in the model corresponded to those of TTI test 405421-1. The

vehicle was given an initial velocity of 101.5 km/hr and it impacted the model just

upstream of a guardrail post at a non-splice location.

4.4.1 Qualitative Validation

The results from the analysis compare well with the results from the full-scale crash test.

Sequential views of the full-scale crash test and simulation are shown in Figures 4.42,

4.43 and 4.44. The longitudinal (forward) velocity-time history of the vehicle during the

impact event is shown in Figure 4.45 and the angular displacement-time histories are

shown in Figures 4.46, 4.47 and 4.48. The acceleration traces in the x-, y- and z-

directions are shown in Figures 4.49, 4.50 and 4.51. The velocity trace of the vehicle in

the F.E. analysis is almost identical to that of the full-scale test until approximately 0.22

seconds, which corresponds to the time of impact of the rear bumper with the w-beam

rail.

The vehicle in the F.E. analysis exits the guardrail at 0.690 second traveling at a speed of

62 km/hr at an angle of 17.8 degrees. The test vehicle exited the system at 0.691 second

traveling at a speed and angle of 55.0 km/hr and 16.0 degrees, respectively. The

maximum roll and pitch angular displacements of the vehicle model in the F.E. analysis

were -8.7 degrees and -3.3 degrees, respectively. The maximum roll and pitch angular

displacements of the test vehicle were -10.1 degrees and -4.3 degrees, respectively. The

continued pitch of the vehicle in the full-scale test at the end of the event, as shown in

Figure 4.47, is due to excessive damage of the wheel assembly which allowed the front of

the vehicle to drop much lower than was case in the F.E. analysis where the wheel

assembly remained in tack. It was not evident from the test video when the wheel

assembly was damaged, but it was likely during impact with either post 14 or post 15.

Damage to the modified G4(1S) guardrail model in the analysis is compared to the damage of the guardrail test installation in Figure 4.52. Posts 13, 14 and 15 were pushed to the ground and the timber blockouts separated from the posts during impact with the front wheel in both the F.E. analysis and the full-scale test. Maximum dynamic deflection of the w-beam rail element was 0.985 m in the F.E. analysis and occurred at a location 0.2 m downstream of post 14. The maximum dynamic deflection of the w-beam rail element reported from the TTI test was 1.0 m and occurred near post 14. The vehicle was in contact with the guardrail over a 9.9-m length of the guardrail in both the F.E. analysis and in the full-scale crash test.

Full-Scale Crash Test Summary - From information provided in the test report, the vehicle impacted the w-beam guardrail 2.5 m upstream of the rail splice at post 13 traveling at 101.5 km/hr at an angle of 25.5 degrees.*(57)* Vehicle redirection began 0.046 second and the front left tire made contact with the front flange of post 13 at 0.107 second. At 0.178 second the front left tire made contact with the front flange of post 14. The rear bumper of the vehicle made contact with the w-beam rail element at 0.225 second. The left front tire of the vehicle made contact with the front flange of post 15 at 0.278 second, as the vehicle became parallel with the guardrail traveling at 68.9 km/hr. At 0.364 seconds the left front tire made contact with the front face of post 16. The vehicle lost contact with the guardrail at 0.691 seconds traveling at a speed of 55 km/hr

160

and at an exit angle of 16 degrees. The maximum dynamic deflection of the guardrail was 1.0 m and the maximum permanent deflection was 0.7 m.

Finite Element Analysis Summary - The vehicle model impacted the modified G4(1S) guardrail model just in front of post 12 at 2.5 m upstream of the rail splice located at post 13 traveling at 101.5 km/hr at an angle of 25.5 degrees. The front left tire made contact with the front flange of post 13 at 0.105 second. At 0.175 second the front left tire made contact with the front flange of post 14. The rear bumper of the vehicle made contact with the w-beam at rail element at 0.205 second. The vehicle became parallel with the rail at 0.270 second traveling at 70 km/hr. The left front tire of the vehicle made contact with the front flange of post 15 at 0.260 second. At 0.355 seconds the left front tire made contact with the front face of post 16. The vehicle lost contact with the guardrail at 0.690 seconds traveling at a speed of 62 km/hr and at an exit angle of 17.8 degrees. At 0.220 seconds the maximum dynamic deflection of the guardrail was 0.985 m and occurred at a location 0.2 m downstream of post 14.

4.4.2   Quantitative Validation

Simulations are generally validated through actual field testing by comparing the field observations to those predicted by the simulation. When agreement is achieved for a particular test (e.g., based on a comparison of various attributes from the model and test, such as path, position, pitch, yaw, roll, accelerations, etc.) the model is considered validated with respect to that test.

Time = 0.000 s

Time = 0.181 s

Time = 0.060 s

Time = 0.360 s

Time = 0.120 s
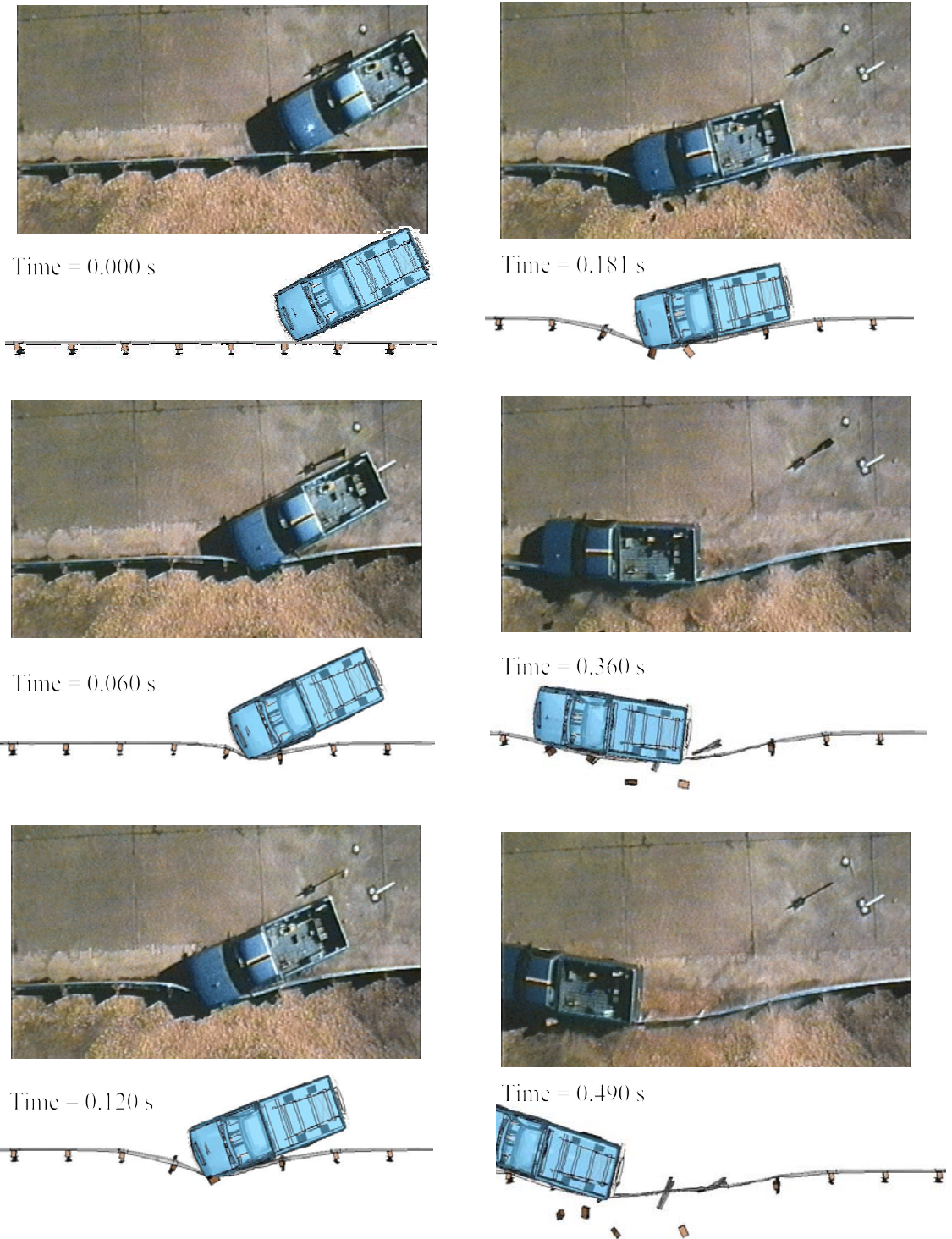
Time = 0.490 s

**Figure 4.42**:   Sequential overhead views of impact event - TTI test 405421-1 and F.E. analysis.
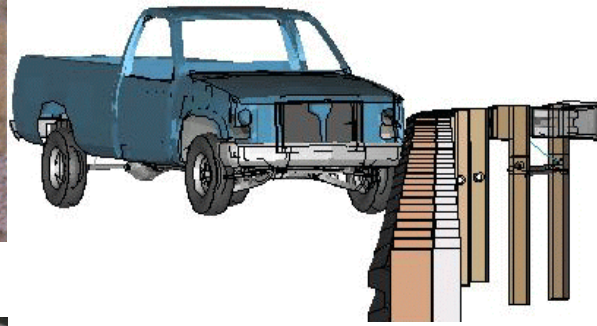
Figure 4.43: Sequential frontal views of impact event - TTI test 405421-1 and F.E. analysis.

Time = 0.360 s
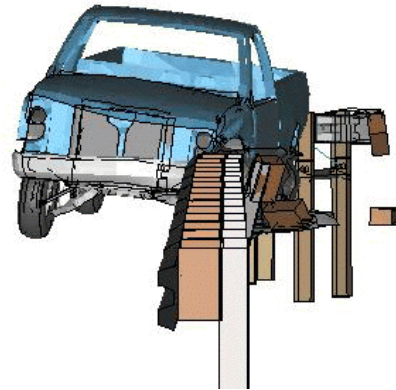
Time = 0.490 s
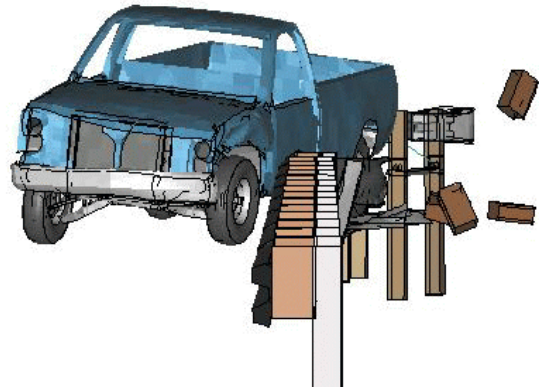
Figure 4.43:   (CONTINUED) Sequential frontal views of impact event - TTI test 405421-1 and F.E. analysis.
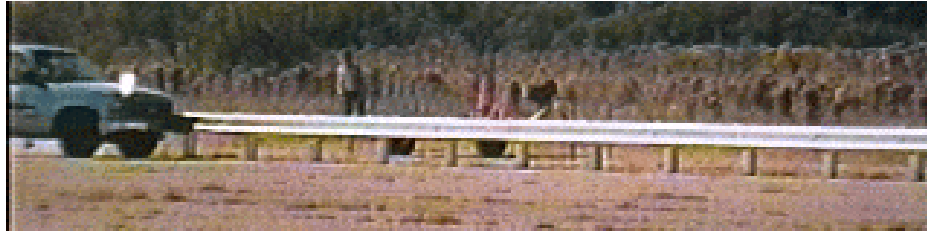
Time = 0.000 s
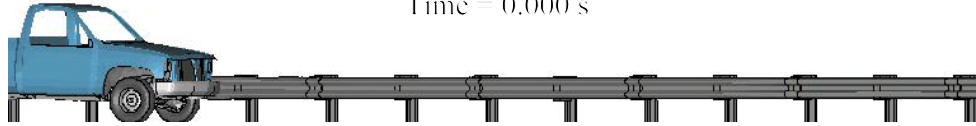
Time = 0.060 s
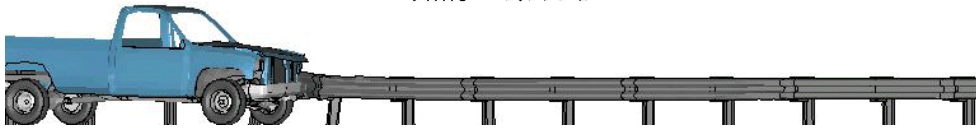
Time = 0.120 s

Figure 4.44:   Sequential oblique views of impact event - TTI test 405421-1 and F.E. analysis.

Time = 0.181 s

Time = 0.360 s

Time = 0.490 s

Figure 4.44:   (CONTINUED) Sequential oblique views of impact event - TTI test
405421-1 and F.E. analysis.

166
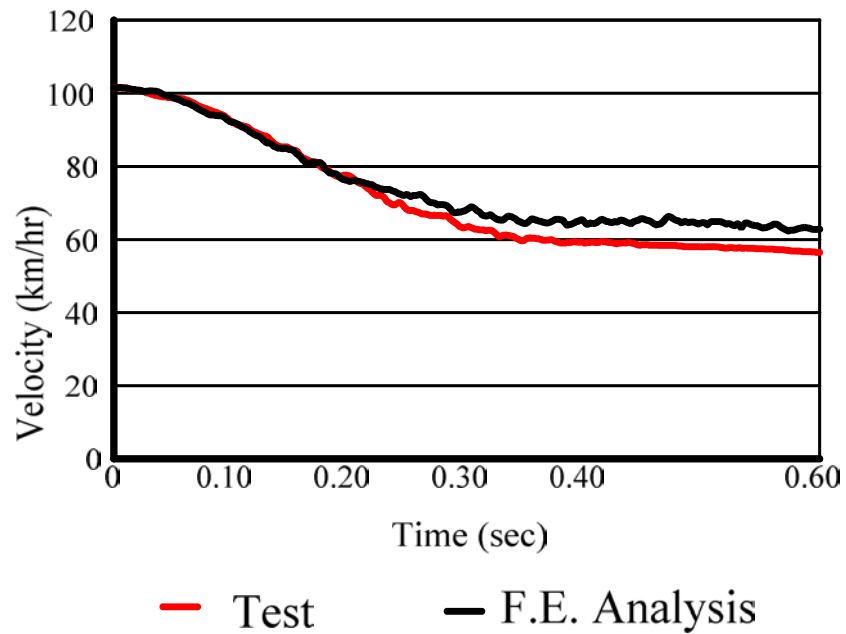
Figure 4.45: Velocity-Time history trace at C.G. of vehicle for TTI
test 405421-1 and F.E. analysis.
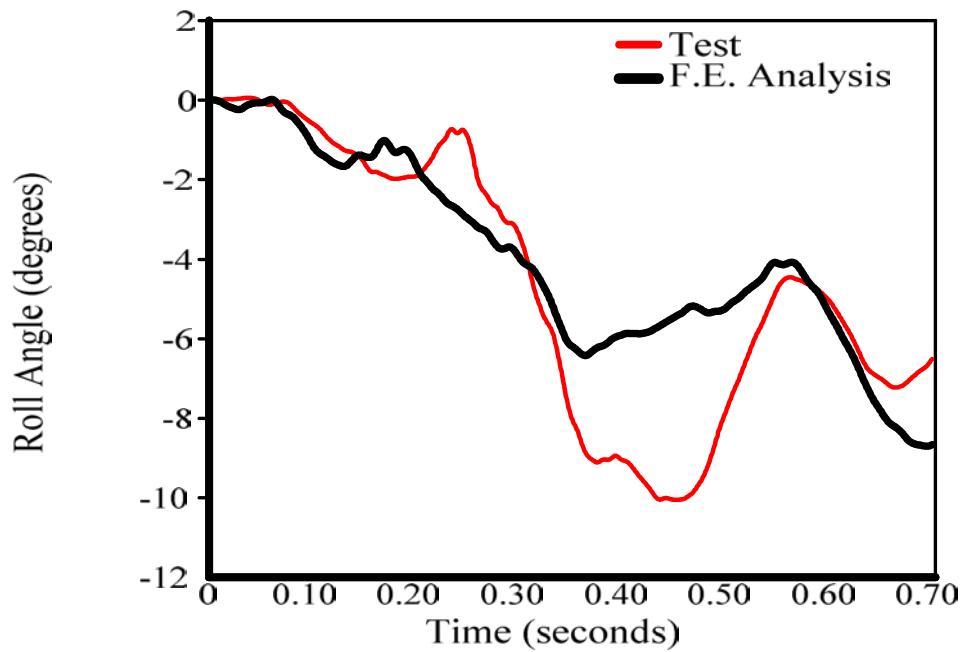
Figure 4.46: Roll angle displacement-time history trace at C.G. of vehicle for
TTI test 405421-1 and F.E. analysis.

167
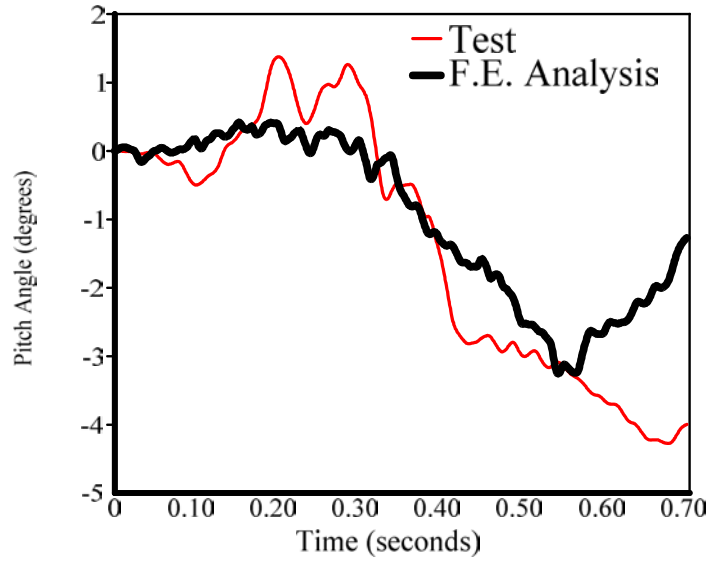
Figure 4.47: Pitch angle displacement-time history trace at C.G. of vehicle for TTI test 405421-1 and F.E. analysis.
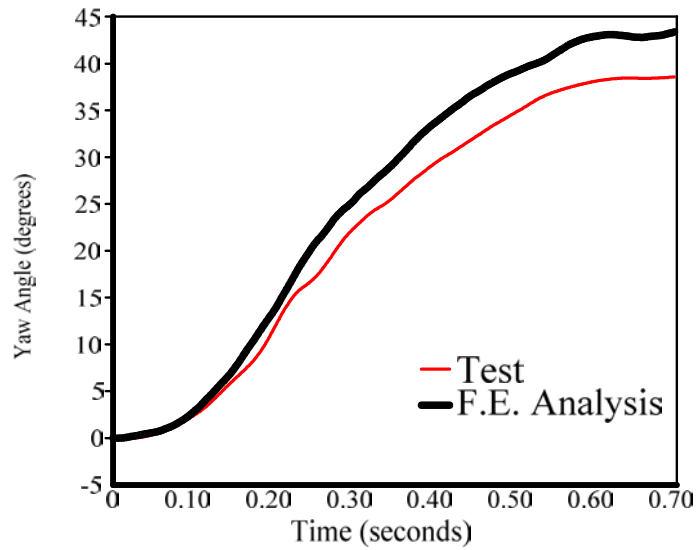
**Figure 4.48**: Yaw angle displacement-time history trace at C.G. of vehicle for TTI test 405421-1 and F.E. analysis.
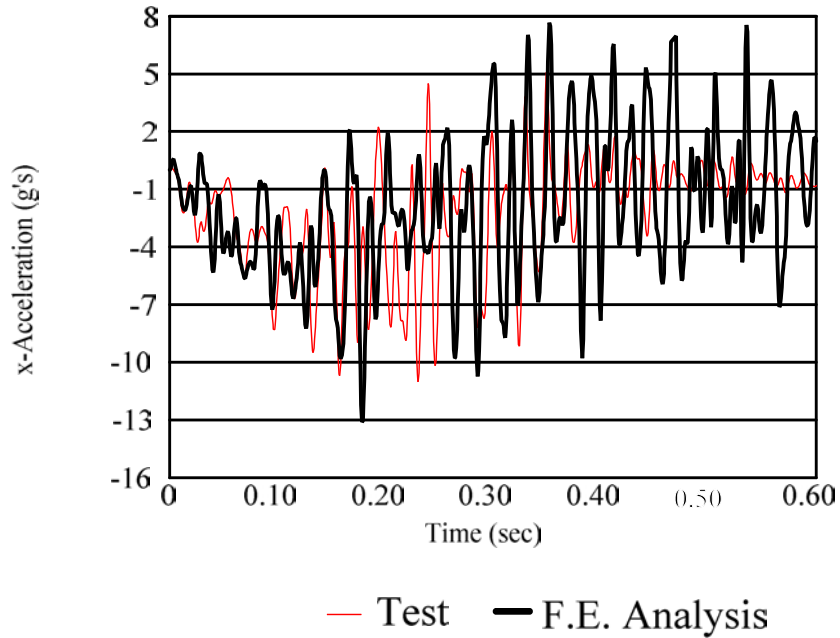
Figure 4.49: Longitudinal acceleration at C.G. of vehicle for TTI test 405421-1 and F.E. analysis - data filtered with SAE class 60 filter.
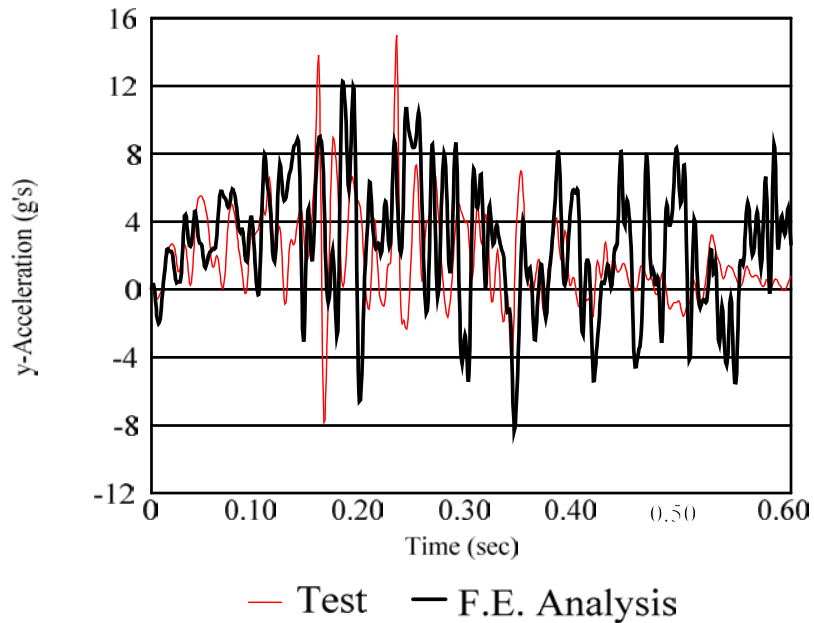
Figure 4.50: Lateral acceleration at C.G. of vehicle for TTI test 405421-1 and F.E. analysis - data filtered with SAE class 60 filter.

169
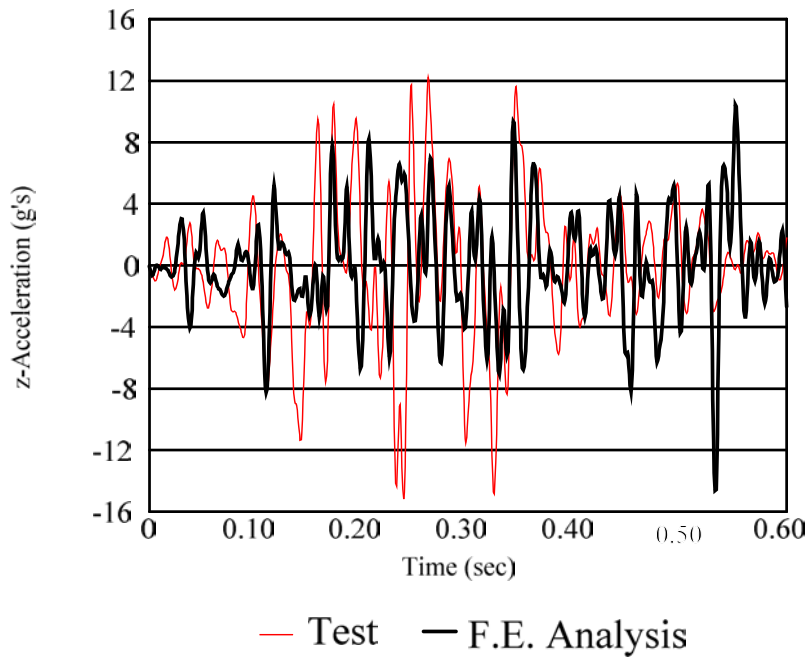
Figure 4.51: Vertical acceleration at C.G. of vehicle for TTI test 405421-1 and F.E. analysis - data filtered with SAE class 60 filter.

TTI Test 405421-1   F.E. Analysis
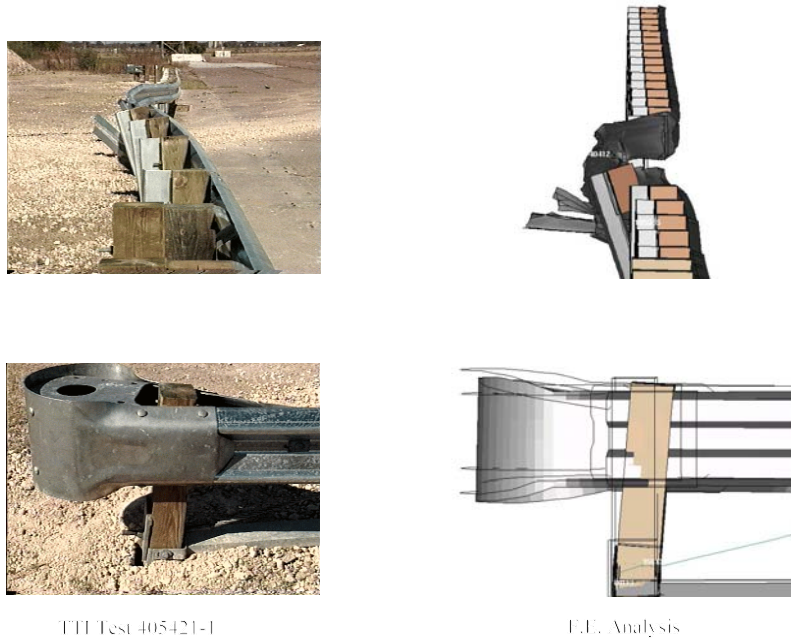
Figure 52: Guardrail damage and anchor movement from TTI test 405421-1 and F.E. analysis.

Often the simulation's predictions are good for some period, but degrade as the simulation continues. For example, a simulation may predict well during the beginning of the modeled event, but degrade with time. The zone over which the model and test are in agreement is referred to as the range of validation. It could be argued that the same is true when comparing two identical full-scale tests. Long-term crash events (i.e., 500-1200 ms) involve numerous factors that can effect the kinematics of the impacting vehicle. With such a high degree of nonlinearity involved in crash events it is often hard to find two seemingly identical full-scale crash tests that are statistically identical over the full extent of the impact event. So it is important to have a realistic model so that the simulation results are at least representative of a possible impact event.

The data was collected from the F.E. analysis in the same manner as it was collected in the full-scale crash test so that a direct comparison of the data could be made. The translational and rotational accelerations of the vehicle model were collected at the center of gravity of the vehicle using the accelerometer option in LS-DYNA in a coordinate frame fixed to the vehicle model, as shown in Figure 4.53 (Note: it was necessary to add some mass to the accelerometer, by increasing the density of the accelerometer material, in order to
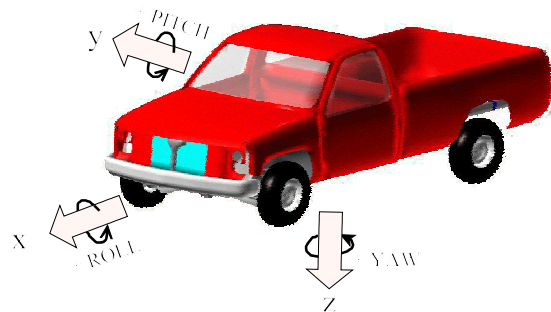

Figure 4.53: Vehicle fixed coordinate reference system.

damp the rigid body noise).

The accelerations at the center of gravity of the vehicle in the simulation and the full-scale test were compared using four quantitative techniques:

      (1) the Test Risk Assessment Program (TRAP),

      (2) the Numerical Analysis of Roadside Design (NARD) validation parameters,

      (3) the analysis of variance method and

      (4) the Geer's parameters.

The TRAP program calculates standardized occupant risk factors from vehicle crash data in accordance with the National Cooperative Highway Research Program (NCHRP) guidelines and the European Committee for Standardization (CEN).*(46)* Since the TRAP program is used to assess full-scale crash test performance, it is useful to compare the TRAP generated parameters to the simulated event. The Numerical Analysis of Roadside Design (NARD) validation procedures are based on concepts of signal analysis and are used for comparing the acceleration-time histories of finite element simulations and full-scale tests.*(43)* The analysis of variance method is a statistical test of the residual error between two signals.*(44)* Geer's method compares the magnitude, phase and correlation of two signals to arrive at a quantitative measure of the similarity of two acceleration-time histories.*(45)* The research team has extensive experience using each of these methods and has routinely included them in their papers and reports on finite element simulation of roadside hardware crashes.

Test Risk Assessment Program (TRAP) Results- The analysis results obtained from TRAP for the full-scale crash test and the F.E. analysis are shown in table 4.11. The table gives the two occupant risk factors recommended by NCHRP Report 350: 1) the lateral and longitudinal components of occupant impact velocity (OIV) and 2) the occupant ridedown acceleration (i.e., the maximum lateral and longitudinal components of resultant vehicle acceleration averaged over 10 ms interval after occupant impact (ORA)). Also given in the table are the CEN risk factors which are the Theoretical Head Impact Velocity (THIV), the Post Impact Head Deceleration (PHD) and the Acceleration Severity Index (ASI). The results indicate that the occupant risk factors for both the full-scale test and the F.E. analysis are similar, however, the occupant risk factors predicted from the F.E. analysis were slightly higher on average than those obtained from the test data.

NARD, Analysis of Variance and Geer's Parameters - The NARD evaluation criteria, analysis of variance results and Geer's parameters were used to determine if the F.E. analysis accurately replicated the results of the full-scale test. Using these criteria, two signals are considered equivalent if the relative absolute difference of moments is less than 0.2, the correlation factor is greater than 0.8 and the Geer's parameters are less than 0.2. Also, the t-statistic of the paired two-tailed t-test of the two signals should be less than the critical 90th percentile value of 2.58.

173

Table 4.11: TRAP results for TTI test 405421-1 and F.E. analysis.

Occupant Risk Factors		Test 405421-1	F.E. Analysis
Occupant Impact Velocity (OIV)	at time (sec)	0.1633	0.1520
	x-direction (m/s)	5.4	4.7
	y-direction (m/s)	-4.4	-5.0
THIV (m/s)		6.3	6.4
Ridedown Acceleration (ORA)	x-direction (g's)	-7.9	-8.9
	y-direction (g's)	8.4	10.0
PHD (g's)		12.1	13.2
ASI		0.68	0.72
Maximum 50 ms moving avg acceleration	x-direction	-5.3 (0.2003 - 0.2503)	-5.2 (0.1137 - 0.1637)
	y-direction	4.3 (0.1483 - 0.1983)	6.0 (0.2037 - 0.2537)

The acceleration-time histories of the analysis were compared to those of the full-scale crash test and the results of the statistical analysis are given in tables 12 and 13. The results in table 4.12 show that the acceleration-time histories compare very well over the first 0.200 seconds of the impact event (which corresponds to the time when the rear bumper contacted the guardrail). The moment differences in the x- and y-directions (longitudinal and transverse directions, respectively) are less than 0.2 (with the exception of the 1st moment difference in the y-direction) indicating very good agreement between test and F.E. analysis over this range of the impact event. The T-statistic in the x-and y-directions also indicate that the test and analysis is in good agreement. The correlation

factors indicates that the x-direction acceleration is in good agreement with the test, however, the y-direction acceleration is somewhat inconsistent. Similarly, the Geer's parameters indicate that the magnitude, phase and correlation of the longitudinal acceleration traces of the test and analysis are in good agreement, while the magnitude and correlation of y-direction acceleration traces are slightly dissimilar.

It is evident in the velocity-time history trace shown in Figure 4.45 that at approximately 0.22 seconds into the simulated impact event that the analysis results were starting to slightly diverge from the test results. This is further confirmed in the statistical analysis results of the full 0.700 seconds of the impact event shown in table 4.13. The moment differences in the x-direction compare well, but are largely in disagreement in the y-direction. The T-statistic also indicates that the x-direction acceleration traces are in good agreement and that the y-direction accelerations are not. The correlation factor is low for both the longitudinal and transverse directions. The Geer's parameters indicate that for the x-acceleration magnitudes are in good agreement while they were slightly out of phase. The Geer's parameters also indicate that the y-direction acceleration traces are not consistent.

4.5   Summary

A finite element model of the modified G4(1S) guardrail with wood blockouts was developed. Due to the immense computational requirements of analyzing a complete guardrail system in geometric and material detail, certain components of the system are

175

Table 4.12: Results of NARD, Analysis of Variance and Geer's Parameters for TTI test 405421-1 and F.E. analysis for the first 0.200 seconds of the impact event.

Comparison Parameters		x-accel. (G's)	y- accel. (g's)
Comparison over 0.200 seconds of impact			
nth Relative Absolute Difference of Moments $\frac{M_n(test)-M_n(analysis)}{M_n(test)}$ (Should be < 0.2)	0th moment difference	0.057 (good)	0.190 (good)
	1st moment difference	0.069 (good)	0.200
	2nd moment difference	0.084 (good)	0.186 (good)
	3rd moment difference	0.104 (good)	0.154 (good)
	4th moment difference	0.128 (good)	0.020 (good)
	5th moment difference	0.158 (good)	0.085 (good)
Correlation Factor (should be > 0.8)		0.863 (good)	0.684
T-Statistic (should be < 2.58)		1.511 (good)	2.22 (good)
Geer's Parameters (should be < 0.2)	Magnitude	0.066 (good)	0.22
	Phase	0.071 (good)	0.173 (good)
	Correlation	0.097 (good)	0.287

Table 4.13: Results of NARD, Analysis of Variance and Geer's Parameters for TTI test 405421-1 and F.E. analysis for the first 0.700 seconds of the impact event.

Comparison Parameters		x-accel. (g's)	y- accel. (g's)
Comparison over 0.700 seconds of impact			
n^{th} Relative Absolute Difference of Moments $\dfrac{M_n(test)\text{-}M_n(analysis)}{M_n(test)}$ (Should be < 0.2)	0th moment difference	0.123 (good)	0.460
	1st moment difference	0.161 (good)	0.650
	2nd moment difference	0.179 (good)	0.912
	3rd moment difference	0.177 (good)	1.23
	4th moment difference	0.160 (good)	1.56
	5th moment difference	0.137 (good)	1.897
Correlation Factor		0.579	0.544
T-Statistic (should be < 2.58)		2.421 (good)	7.4
Geer's Parameters (should be < 0.2)	**Magnitude**	0.176 (good)	0.418
	Phase	0.239	0.262
	Correlation	0.297	0.493

modeled using simpler methods. The details of the modeling methodology for each component of the modified G4(1S) guardrail was provided in the preceding sections.

The finite element model of the modified G4(1S) guardrail was validated by simulating a crash test that was conducted at Texas Transportation Institute. The NCAC version 9 C2500 vehicle model with modifications to the suspension system was used to simulate the vehicle in the crash test. There was good agreement between the test and simulation with respect to velocity histories, event timing, exit conditions, guardrail damage, guardrail deflections, as well as the TRAP and NARD evaluation parameters in the longitudinal direction. The results of the finite element analysis were determined to be statistically equivalent to the results of the full-scale test over the first 0.200 seconds of the impact event. The results of the finite element analysis were also very similar to that of the full-scale test in the x-direction over the full 0.700 seconds of impact, however, the y-direction results were somewhat in error.

4.6   Conclusions

The results of the simulation were compared to the full-scale crash test and the model was validated both qualitatively and quantitatively. The finite element model replicates the basic phenomological behavior of the system in a redirectional impact with a 2000-kg pickup truck. One major difference between the test and simulation results was that the wheel assembly of the vehicle in the full-scale test was severely damaged and pushed back under the vehicle. In the finite element analysis the wheel impacted posts 13, 14, 15

and 16, however, the wheel assembly remained in tact. The position of the front wheel during impact with the posts in the finite element analysis, as well as the position of the posts resulted in lower impact forces and ultimately less damage to the wheel assembly. The event of wheel assembly damage or failure during impact can have a significant affect on the kinematics of a vehicle in the latter stages of redirection which was the case in this study. It is believed, however, that results of the analysis are reasonable and present realistic behavior of both the guardrail and vehicle in such an impact and that the models can be used with confidence to investigate the response of the system under various impact conditions.